TWO-LOOP RADIATIVE CORRECTIONS OF ELECTROWEAK MIXING ANGLE AND BRANCHING FRACTION FOR $Z \to B\bar{B}$

by

Yi-Cheng Huang

Bachelor's degree, National Taiwan University, 1997

Master's degree, National Tsing-Hua University, 1999

Submitted to the Graduate Faculty of

the Department of Physics and Astronomy in partial fulfillment

of the requirements for the degree of

Doctor of Philosophy

University of Pittsburgh

2012

UNIVERSITY OF PITTSBURGH

DEPARTMENT OF PHYSICS AND ASTRONOMY

This dissertation was presented

by

Yi-Cheng Huang

It was defended on

July 25th 2012

and approved by

Ayres Freitas, Department of Physics and Astronomy

Eric Swanson, Department of Physics and Astronomy

James Mueller, Department of Physics and Astronomy

Robert Devaty, Department of Physics and Astronomy

Ira Rothstein, Department of Physics, Carnegie Mellon University

Dissertation Director: Ayres Freitas, Department of Physics and Astronomy

TWO-LOOP RADIATIVE CORRECTIONS OF ELECTROWEAK MIXING ANGLE AND BRANCHING FRACTION FOR $Z \to B\bar{B}$

Yi-Cheng Huang, PhD

University of Pittsburgh, 2012

In this thesis I develop a numerical technique which is based on the Mellin-Barnes representation to calculate two-loop Feynman integrals. The resulting complex integrals of high dimensions are being applied with some treatments, such as the variable transform, reduction formulas, etc, to improve the convergence of the integrals. The approach is adopted to compute the two-loop radiative corrections of the electroweak mixing angle, $\sin\theta_W$, and the hadronic branching ratio R_b for the process $Z \to b\bar{b}$. I focus on contributions with an internal fermion sub-loop using the on-shell renormalization scheme. The results will help to derive improved constraints on the Higgs particle.

TABLE OF CONTENTS

LIST OF TABLES

LIST OF FIGURES

1.0 INTRODUCTION

Currently, the theory for particle physics is called the Standard Model (SM), which describes the electromagnetic, weak and strong nuclear interactions through the dynamics of mediating particles. Through the progress of the high precision measurements in accelerator laboratories for the past years, the SM has been stringently tested, for example, the determination of the number of light neutrinos, mass measurements of the weak gauge bosons, such as the Z-boson, etc. With the improvement of the precision, the results of the experiments could shed more light on the physics beyond our current knowledge in particular at the higher energy scales. For instance, the only missing part in the SM is the Higgs particle, which gives the masses to the rest of the particles except itself, and its existence could be unveiled through the high precision measurements, such as the mass of the W-boson, the electroweak mixing angle $\sin\theta_W$, etc. At present, the experimental value of W-boson mass, $M_W^{\rm exp}$, is around 80.398 GeV with an error $3 \times 10^{-4} (\delta M_W = 23\,\text{MeV})$ [1]. Theoretically, the mass of the W-boson is predicted by the SM in the muon decay through the formula

$$M_W^2 = \frac{M_Z^2}{2}\left(1 + \sqrt{1 - \frac{4\pi\alpha}{\sqrt{2}G_F M_Z^2}(1+\Delta r)}\right), \tag{1.1}$$

where Δr contains the radiative corrections [2]. Experimentally, the precisions of the Fermi constant G_F and the mass of Z-boson can reach 10 times better than that of the W-boson, so they are used as input parameters in the prediction.

Theoretically, one-loop radiative corrections in Δr would contribute around 1.5×10^{-3} to the mass and two-loop ones would give about 3×10^{-4} [3] depending on the mass of the Higgs particle. When comparing with the expected error of W-boson mass in LHC, 1.9×10^{-4} (15 MeV) [4], it is clear that two-loop radiative corrections play an important role

in constraining the Higgs sector. Besides the W mass, the effective weak mixing angle $\sin^2\theta_{\rm eff}$ is another precision observable that constrains the SM and the Higgs mass. It parametrizes the couplings of the Z-boson to left- and right-handed fermions. For leptons the complete two-loop corrections are known. The experimental error for the $\sin^2\theta_{\rm eff}^{\rm lept}$ is about 1.7×10^{-4} [1], while its theoretical correction of the next-to-next-leading order (NNLO) [5] is roughly the same size. As the goal of this project, I intended to work on the two-loop calculations for the b quarks in the Z boson decay. The dominant two-loop corrections from closed fermion loops in the computations of $\sin^2\theta_{\rm eff}^{b\bar{b}}$ [6] have been done recently, therefore parts of this work are to generate consistent results. Another goal is to calculate the branching ratio of the b quarks in the Z boson decay, R_b [7, 8], whose two-loop radiative contributions have not been completed before this work.

In general the two-loop integrals cannot be integrated analytically due to multiple mass and momentum scales, so that the development of numerical methods is important in computing these integrals. The Mellin-Barnes (MB) representation is the method which has a general way to isolate the singularities of arbitrary multi-loop integrals, unlike other efficient methods, such as the Dispersion Relation, which are limited to certain types of diagrams. The goal of this research is to improve the numerical precision by using the MB and see how its applications can improve the computations of the physical observables. In the following chapter, a brief introduction of the SM for the electroweak theory is provided, and the relations between the Lagrangian and the gauge principle are discussed. In addition, an investigation of how the experimental observables are related to theoretical parameters is presented. For this thesis, the on-shell renormalization scheme is adopted and the corresponding counterterms and the renormalization conditions are depicted in the third chapter. In the fourth chapter, the numerical method based on the Mellin-Barnes representation and the integration techniques that we have developed are discussed as well as other approaches which are summarized for a general understanding. The issues related to calculating the two-loop radiative corrections for the electroweak mixing angle for $Z\to b\bar{b}$ as well as the $Z\to b\bar{b}$ branching fraction, R_b, are explained in the fourth section, including the use of the software, the reduction method of the tensor integrals, etc. In chapter 6, the results of the computations are presented and the conclusions are provided in the last chapter.

2.0 ELECTROWEAK MODEL AND EXPERIMENTAL TESTS

2.1 ELECTROWEAK STANDARD MODEL

As to the electroweak interactions, the Glashow-Salam-Weinberg model gives the most satisfying predictions for the current experimental results. By taking a deeper view, the spirit that resides in the SM is Gauge Invariance (GI), and it becomes a principle that runs through the whole theory. The Classical Lagrangian $\mathcal{L}_C$ of the SM includes a Yang-Mills part, a Higgs part and a fermion part

$$\mathcal{L}_C = \mathcal{L}_{YM} + \mathcal{L}_H + \mathcal{L}_F. \tag{2.1}$$

The Yang-Mills part depicts the fields of gauge bosons,

$$\mathcal{L}_{YM} = -\frac{1}{4}(\partial_\mu W^a_\nu - \partial_\nu W^a_\mu + g_2 \epsilon^{abc} W^b_\mu W^c_\nu)^2 - \frac{1}{4}(\partial_\mu B_\nu - \partial_\nu B_\mu)^2, \tag{2.2}$$

where ϵ^{abc} are the totally antisymmetric structure constants of SU(2).

For the Higgs part and the fermion part, the covariant derivative, D_μ, with respect to the Higgs particle or fermions generates the interactions with gauge bosons:

$$D_\mu = \partial_\mu - i g_2 I^a W^a_\mu + i g_1 \frac{Y_W}{2} B_\mu, \tag{2.3}$$

where g_1 and g_2 are the coupling constants for the respective gauge bosons B_μ of $\mathrm{U}(1)_Y$ and W^a_μ of $\mathrm{SU}(2)_W$. The electric charge operator Q is given by the Gell-Mann Nishijima relation,

$$Q = I^3_W + \frac{Y_W}{2}, \tag{2.4}$$

where the eigenvalues of the weak isospin generator I^3_W and the weak hypercharge Y_W for various particles are assigned with rational values to ensure the gauge invariance.

In the SM, the masses of the particles are created due to the symmetry breaking of a Higgs particle. The particle is a complex scalar $\mathrm{SU}(2)_W$ doublet field with hypercharge $Y_W = 1$, and the Lagrangian $\mathcal{L}_H$ is as below

$$\mathcal{L}_H = (D_\mu \Phi)^\dagger (D^\mu \Phi) - V(\Phi), \tag{2.5}$$

where $\Phi(x) = \begin{bmatrix} \phi^\dagger(x) \\ \phi^0(x) \end{bmatrix}$ and the potential $V(\Phi) = \frac{\lambda}{4}(\Phi^\dagger\Phi)^2 - \mu^2 \Phi^\dagger\Phi$. The parameters λ and μ are chosen to give a nonzero vacuum expectation value, v, for the Higgs field, $|\langle 0|\Phi|0\rangle|^2 = \frac{2\mu^2}{\lambda} = \frac{v^2}{2} \neq 0$, in order to generate the masses of the particles. In the broken phase, the Higgs sector is in the form of

$$\Phi(x) = \begin{bmatrix} \phi^+(x) \\ \frac{1}{\sqrt{2}}(v + H(x) + i\chi(x)) \end{bmatrix}, \tag{2.6}$$

where the components ϕ^+ and χ are the unphysical degrees of freedom and can be eliminated by fixing a specific gauge. $H(x)$ is the only physical field and carries a mass $M_H = \sqrt{2}\mu$.

For the fermion part, the left-handed and right-handed leptons and quarks transform differently as $\mathrm{SU}(2)_W$ doublets and singlets

$$\begin{aligned} &L_j^L = \omega_- L_j = \begin{bmatrix} \nu_j^L \\ l_j^L \end{bmatrix}, Q_j^L = \omega_- Q_j = \begin{bmatrix} u_j^L \\ d_j^L \end{bmatrix}, \\ &l_j^R = \omega_+ l_j, \quad u_j^R = \omega_+ u_j, \quad d_j^R = \omega_+ d_j, \end{aligned} \tag{2.7}$$

where $\omega_\pm = \frac{1 \pm \gamma_5}{2}$. The fermion part of the Lagrangian reads

$$\begin{aligned} \mathcal{L}_F &= \sum_i (\bar{L}_i^L i\gamma^\mu D_\mu L_i^L + \bar{Q}_i^L i\gamma^\mu D_\mu Q_i^L) \\ &+ \sum_i (\bar{l}_i^R i\gamma^\mu D_\mu l_i^R + \bar{u}_i^R i\gamma^\mu D_\mu u_i^R + \bar{d}_i^R i\gamma^\mu D_\mu d_i^R) \\ &- \sum_{ij} (\bar{L}_i^L G_{ij}^l l_i^R \Phi + \bar{Q}_i^L G_{ij}^u u_j^R \Phi + \bar{d}_i^L G_{ij}^d d_i^R \Phi + h.c.), \end{aligned} \tag{2.8}$$

where G_{ij}^l, G_{ij}^u and G_{ij}^d are the Yukawa coupling matrices. By taking the minimal value of the potential $V(\Phi)$ for the Higgs field at $|\langle\Phi\rangle| = \frac{v}{\sqrt{2}}$, the masses of the fermions are generated while preserving GI . For a complete calculations of a physical process, in addition to the classical Lagrangian, one needs a gauge fixing term to specify a gauge, and a Faddeev Popov

ghost Lagrangian to ensure the gauge invariance of the theory [9]. A 'tHooft gauge is chosen with

$$\begin{aligned} F^{\pm} &= (\xi_1^W)^{-\frac{1}{2}}\partial^\mu W_\mu^{\pm} \mp iM_W(\xi_2^W)^{\frac{1}{2}}\phi^{\pm}, \\ F^Z &= (\xi_1^Z)^{-\frac{1}{2}}\partial^\mu Z_\mu^{\pm} - M_Z(\xi_2^Z)^{\frac{1}{2}}\chi, \\ F^\gamma &= (\xi_1^\gamma)^{-\frac{1}{2}}\partial^\mu A_\mu. \end{aligned} \tag{2.9}$$

for the gauge fixing Lagrangian

$$\mathcal{L}_{\text{fix}} = -\frac{1}{2}\left[(F^\gamma)^2 + (F^Z)^2 + 2F^+F^-\right], \tag{2.10}$$

where ξ_1^X and ξ_2^X $(X = W, Z)$ are the gauge fixing constants. However the gauge fixing Lagrangian is not gauge invariant so that it contains unphysical effects that have to to be removed from the calculations. Thus, it can be proved that by adding an extra Faddeev Popov ghost Lagrangian

$$\mathcal{L}_{\text{FP}} = \bar{u}(x)\frac{\delta F^\alpha}{\delta\theta^\beta(x)}u^\beta(x), \tag{2.11}$$

where $\theta(x)$ is an infinitesimal gauge transformation for the fixing operators F^α $(\alpha = \pm, \gamma, Z)$, the sum $\mathcal{L}_{\text{fix}} + \mathcal{L}_{\text{FP}}$ are invariant under a generalized type of gauge trandformations called BRST transformation [9]. Therefore we can obtain the total Lagrangian for the GSW theory which reads

$$\mathcal{L}_{GSW} = \mathcal{L}_C + \mathcal{L}_{\text{fix}} + \mathcal{L}_{\text{FP}}. \tag{2.12}$$

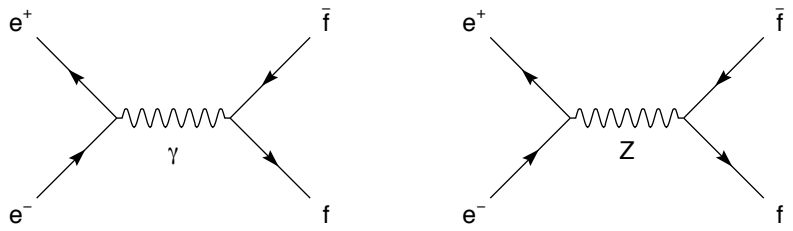

Figure 1: The lowest-order s-channel Feynman diagrams for $e^+e^- \to f\bar{f}$

2.2 ELECTROWEAK PRECISION TESTS AND THEORY

2.2.1 The Z resonance

With the observations of the W and Z bosons in 1983, the electroweak theory was well confirmed experimentally. The production of the Z boson proceeds via the fermion and anti-fermion annihilation, such as $e^+e^- \to f\bar{f}$. The LEP and SLAC e^+e^- accelerators have accumulated copious data for the measurements of the Z boson with high precision. The s-channel of the e^+e^- annihilation through a virtual photon exchange in the left Figure 1 gives rise to the $1/s$ fall-off and a peak at the low energies in the hadronic cross-section plot, Figure 2. The exchange of the Z boson in the right of the Figure 1 leads to another peak at the 91 GeV. In the SM, the electroweak corrections to the couplings of the Z boson is absorbed into complex form factors, $\mathcal{R}_f$ for the overall coupling strength and $\mathcal{K}_f$ for the relative strength of the vector and axial-vector couplings; the vector and axial-vector couplings are described by

$$\begin{aligned} g_{Vf} &= \sqrt{\mathcal{R}_f}(T_3^f - 2Q_f\mathcal{K}_f \sin^2\theta_W), \\ g_{Af} &= \sqrt{\mathcal{R}_f}T_3^f, \end{aligned} \tag{2.13}$$

where Q_f and T_3^f are the charge and the third component of the weak isospin of the fermion. Without taking into account of the initial and final state photon radiation, final state gluon radiation and fermion masses, the differential cross-section for fermion pair production around the Z resonance for the unpolarized electrons can be described by the the complex-value effective coupling constants in (2.13) in the Born-type structure,

$$\begin{aligned} \frac{2s}{\pi}\frac{1}{N_c^f}\frac{d\sigma_{ew}}{d\cos\theta_W}(e^+e^- \to f\bar{f}) &= |\alpha(s)Q_f|^2(1+\cos^2\theta) \\ &-8\Re\left\{\alpha^*(s)Q_f\chi(s)\left[g_{Ve}g_{Vf}(1+\cos^2\theta)+2g_{Ae}g_{Af}\cos\theta\right]\right\} \\ &+16|\chi(s)|^2\left[(|g_{Ve}|^2+|g_{Ae}|^2)(|g_{Vf}|^2+|g_{Af}|^2)(1+\cos^2\theta)\right. \\ &\left.+8\Re\{g_{Ve}g_{Ae}^*\}\Re\{g_{Vf}g_{Af}^*\}\cos\theta\right], \end{aligned} \tag{2.14}$$

where $\chi(s) = \frac{G_F m_Z^2}{8\pi\sqrt{2}} \frac{s}{s - M_Z^2 + is\Gamma_Z/M_Z}$, $N_c^{\rm f}$ is the colour factor of the fermion and θ is the scattering angle of the out-going fermion with respect to the direction of the ingoing electron. The cross-section contains three contributions from s-channel γ exchange, the $\gamma - Z$ interference term and s-channel Z exchange, as shown from the first, second, and last two lines of (2.14). The partial Z decay widths can be written with QED and QCD final state [12, 14] corrections as

$$\Gamma_{\rm f\bar{f}} = N_c^{\rm f} \frac{G_{\rm F} M_Z^3}{6\sqrt{2}\pi} \left(|g_{\rm Af}|^2 R_{\rm Af} + |g_{\rm Vf}|^2 R_{\rm Vf} \right).$$

The radiator factors $R_{\rm Af}$ and $R_{\rm Vf}$ take into account the final state QED and QCD corrections. To the leading order, they are given by

$$R_{\rm A,QCD} = R_{\rm V,QCD} = 1 + \frac{\alpha_S(M_Z^2)}{\pi} + \cdots, \tag{2.15}$$

and

$$R_{\rm A,QED} = R_{\rm V,QED} = 1 + \frac{3}{4} Q_{\rm f}^2 \frac{\alpha(M_Z^2)}{\pi} + \cdots. \tag{2.16}$$

In principle, the total cross-section can be written in terms of the partial decay widths of the initial and final states, $\Gamma_{\rm ee}$ and $\Gamma_{\rm f\bar{f}}$, namely the Breit-Weigner formula,

$$\sigma_{\rm f\bar{f}}^Z = \sigma_{\rm f\bar{f}}^0 \frac{s\Gamma_Z^2}{(s - M_Z^2)^2 + s^2\Gamma_Z^2/M_Z^2}, \tag{2.17}$$

where

$$\sigma_{\rm f\bar{f}}^0 = \frac{12\pi}{M_Z^2} \frac{\Gamma_{\rm ee}\Gamma_{\rm f\bar{f}}}{\Gamma_Z^2}, \tag{2.18}$$

if s-channel γ exchange is ignored. The total width of Z decays in (2.17) due to the instability of the Z boson contains the partial widths as below

$$\Gamma_Z = \Gamma_{ee} + \Gamma_{\mu\mu} + \Gamma_{\tau\tau} + \Gamma_{\rm had} + \Gamma_{\rm inv}, \tag{2.19}$$

where this hadronic width is given by the sum of all quark final states except the top quark $\Gamma_{\rm had} = \sum_{q \neq t} \Gamma_{\rm q\bar{q}}$. The invisible width from Z decays to neutrinos, $\Gamma_{\rm inv} = N_\nu \Gamma_{\nu\bar{\nu}}$, where N_ν is the number of the neutrino generations, can be determined from (2.19) by measuring Γ_Z from the shape of Figure 2 and the visible partial widths from the cross-sections in (2.18). In Figure 3, it illustrates a strong constraint on N_ν from the measurements of the hadronic peak cross-section; N_ν, other than three neutrino species, is severely suppressed.

To summarize, the parameters that describe the total hadronic and leptonic cross-section around the Z peak are: the mass of the Z, M_Z, the total width Γ_Z, the hadronic pole cross-section,

$$\sigma_{\rm had}^0 \equiv \frac{12\pi}{M_Z^2} \frac{\Gamma_{\rm ee}\Gamma_{\rm had}}{\Gamma_Z^2},$$

and the ratios

$$R_{\rm e}^0 \equiv \Gamma_{\rm had}/\Gamma_{\rm ee},\ R_\mu^0 \equiv \Gamma_{\rm had}/\Gamma_{\mu\mu},\ R_\tau^0 \equiv \Gamma_{\rm had}/\Gamma_{\tau\tau} \text{ and } R_b^0 \equiv \Gamma_{\rm had}/\Gamma_{\rm bb},$$

which are determined from the measurements of the experiments. All corrections from s-channel photon exchange and initial and final state QED and QCD correction can be included in a numerical program, such as ZFitter [10], GFitter [11], etc. The theoretical computation of the branching fraction R_b so far is finished up to one-loop corrections [7, 8] with final-state QED and QCD corrections of order $\mathcal{O}(\alpha_s^2, \alpha_s^3, \alpha\alpha_s)$ [12], and in this work the electroweak two-loop corrections will be performed.

2.2.2 The measurements of electroweak couplings

The SM is a highly tested theory in particle physics by the experiments that are performed in accelerator laboratories, such as Tevatron, LEP etc [13]. Thus, an understanding of how the measurements relate to parameters in the SM, like masses, coupling constants etc, is important. From the GSW theory as mentioned above, the Z-boson coupling constants can be divided into the left and right-handed ones, $g_{\rm Lf}$ and $g_{\rm Rf}$ with respect to the chiral properties of the fermions. Alternatively, the vector and axial coupling constants can be defined as follows,

$$g_{\rm Vf} \equiv g_{\rm Lf} + g_{\rm Rf} \quad \text{and} \quad g_{\rm Af} \equiv g_{\rm Lf} - g_{\rm Rf}. \tag{2.20}$$

The effective electroweak mixing angle is defined through the ratio of the vector and axial coupling constants

$$\frac{g_{\rm Vf}}{g_{\rm Af}} = 1 - \frac{Q_{\rm f}}{T_3^{\rm f}} \sin^2\theta_{\rm eff}^{\rm f} = 1 - 4|Q_{\rm f}| \sin^2\theta_{\rm eff}^{\rm f}, \tag{2.21}$$

or equivalently: $\sin^2\theta_{\rm eff}^{\rm f} \equiv \frac{1}{4}(1 + \frac{g_{\rm Vf}}{g_{\rm Af}})$. At Born level, $g_{\rm Vf}$ and $g_{\rm Af}$ are given by

$$g_{\rm Vf} \equiv (T_{\rm f}^3 - 2Q_{\rm f} \sin^2\theta_{\rm eff}^{\rm f}), \;\; g_{\rm A} \equiv T_{\rm f}^3. \tag{2.22}$$

Beyond Born level, the coupling constants, $g_{\rm Vf}$ and $g_{\rm Af}$, contain the radiative corrections, and lots of work in calculations of the weak mixing angles for different decay products has been done lately, such as $\sin^2\theta_{\rm eff}^{\rm lept}$ [5], $\sin^2\theta_{\rm eff}^{\rm b\bar{b}}$ [6], etc., as well as the final-state QCD and QED corrections of order $\mathcal{O}(\alpha\alpha_s)$ [12] and $\mathcal{O}(\alpha\alpha_s^2)$ [14]. As for higher order corrections, such as $\mathcal{O}(\alpha\alpha_s)$, $\mathcal{O}(\alpha\alpha_s)$, $\mathcal{O}(\alpha\alpha_s)$ [15], their contributions are proved to be very small. A one-loop example is shown in Figure 4, which involves a Higgs boson interacting in the decay process; this is the way that we could constrain the mass of the Higgs through the precision measurements of the SM.

Experimentally, the weak mixing angle and the branching frations are determined from measuring the cross-section of $\rm e^+e^- \to Z \to f\bar{f}$ for different final states, as a function of the scattering angle θ, the initial beam polarization, etc. For the process $\rm e^+e^- \to f\bar{f}$ with Z exchange only, the Born level differential cross section with unpolarized final states is

$$\frac{{\rm d}\sigma_{\rm f\bar{f}}}{{\rm d}\cos\theta} = \frac{3}{8}\sigma_{\rm f\bar{f}}^{\rm tot}\left[(1 - \mathcal{P}_{\rm e}\mathcal{A}_{\rm e})(1 + \cos^2\theta) + 2(\mathcal{A}_{\rm e} - \mathcal{P}_{\rm e})\mathcal{A}_{\rm f}\cos\theta\right]. \tag{2.23}$$

The electron beam polarization $\mathcal{P}_{\rm e}$ is positive for right-handed beam helicity, negative for left-handed. The dependence of the fermion couplings is described by the convenient asymmetry parameters, $\mathcal{A}_{\rm f}$, as below

$$\mathcal{A}_{\rm f} = \frac{g_{\rm Lf}^2 - g_{\rm Rf}^2}{g_{\rm Lf}^2 - g_{\rm Rf}^2} = 2\frac{g_{\rm Vf}/g_{\rm Af}}{1 + (g_{\rm Vf}/g_{\rm Af})^2} \tag{2.24}$$

$$= \frac{1 - 4|Q_{\rm f}| \sin^2\theta_{\rm eff}^{\rm f}}{1 - 4|Q_{\rm f}| \sin^2\theta_{\rm eff}^{\rm f} + 8Q_{\rm f}^2 \sin^4\theta_{\rm eff}^{\rm f}}, \tag{2.25}$$

and it is clear that it only depends on the ratio of the couplings. Experimentally, the asymmetry parameters can be extracted from the measured asymmetry observables.

$$
\begin{aligned}
A_{\rm FB} &\equiv \frac{\sigma_F - \sigma_B}{\sigma_F + \sigma_B}, \\
A_{\rm LR} &\equiv \frac{\sigma_L - \sigma_R}{\sigma_L + \sigma_R}\frac{1}{\langle|\mathcal{P}_e|\rangle}, \\
A_{\rm LRFB} &\equiv \frac{(\sigma_F - \sigma_B)_L - (\sigma_F - \sigma_B)_R}{(\sigma_F + \sigma_B)_L + (\sigma_F + \sigma_B)_R}\frac{1}{\langle|\mathcal{P}_e|\rangle}, \\
\langle\mathcal{P}_\tau\rangle &\equiv \frac{\sigma_{\rm r} - \sigma_{\rm l}}{\sigma_{\rm r} + \sigma_{\rm l}}, \\
A_{\rm FB}^{\rm pol} &\equiv \frac{(\sigma_{\rm r} - \sigma_{\rm l})_{\rm F} - (\sigma_{\rm r} - \sigma_{\rm l})_{\rm B}}{(\sigma_{\rm r} + \sigma_{\rm l})_{\rm F} + (\sigma_{\rm r} + \sigma_{\rm l})_{\rm B}},
\end{aligned}
$$

where the subscripts F and B designate the integrals over forward and backward hemispheres, L and R for left and right electron helicities and l and r for left and right fermion helicities. Simply by inspection of (2.23), the relations between the cross section asymmetries and the asymmetry parameters of fermions are obtained as follows

$$
\begin{aligned}
A_{\rm FB}^{\rm f} &= \frac{3}{4}\mathcal{A}_{\rm e}\mathcal{A}_{\rm f}, \\
A_{\rm LR} &= \mathcal{A}_{\rm e}, \\
A_{\rm LRFB} &= \frac{3}{4}\mathcal{A}_{\rm f}, \\
\langle\mathcal{P}_\tau\rangle &= -\mathcal{A}_\tau, \\
A_{\rm FB}^{\rm pol} &= -\frac{3}{4}\mathcal{A}_{\rm e}.
\end{aligned}
$$

Using $\mathcal{A}_e$ as determined from $A_{\rm LR}$, the parameters $\mathcal{A}_\mu$, $\mathcal{A}_\tau$, etc., can be inferred independently from the forward and backward asymmetry measurements. Thus, the various asymmetries provide information about the ratio of couplings $g_{\rm Vf}/g_{\rm Af}$, while the total coupling strength for the $Z \to f\bar{f}$ interaction can be inferred from the cross-section $\sigma_{\rm f\bar{f}}$ and branching ratios R_b.

As examples of how the radiative corrections play a role in the prediction of physical observables, the analyses of the experimental and the theoretical results [1] demonstrate the constraints on the Higgs masses in Figure 5. Another example of the radiative corrections for the prediction of the Higgs sector through M_W is present in Figure 6. In the figure, the next-to-leading order and the next-to-next-to-leading order radiative corrections of M_W through Δr [3], as in (1.1), is affected by the mass of the Higgs, and it shows the small mass of the Higgs, near 100 GeV, is preferred in precision tests of the SM.

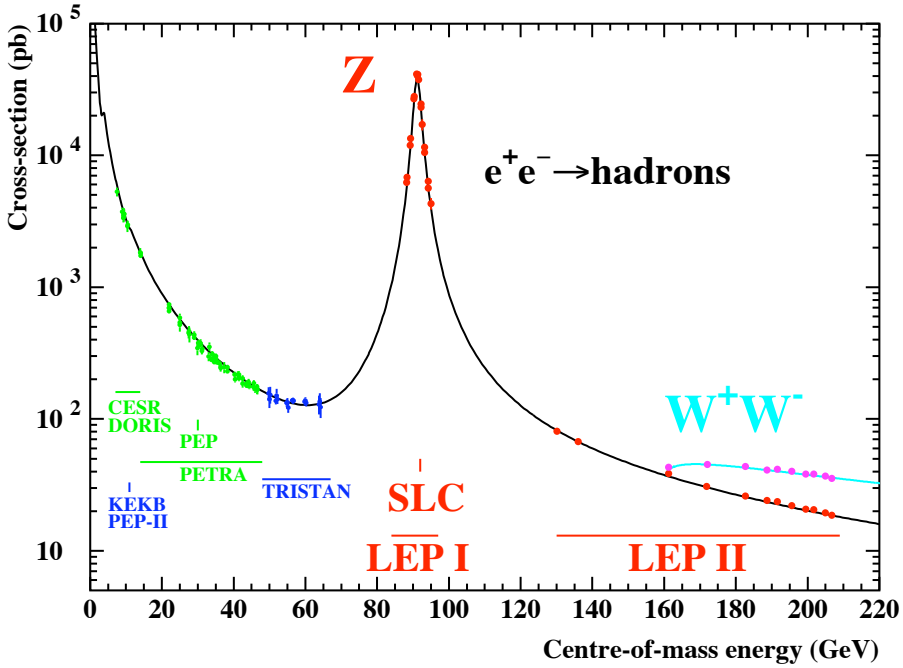

Figure 2: The hadronic cross-section as a function of centre-of-mass energy. The solid line is the prediction of the SM, and the points are the experimental measurements. Also indicated are the energy ranges of various e^+e^- accelerators. The cross-sections have been corrected for the effects of photon radiation.

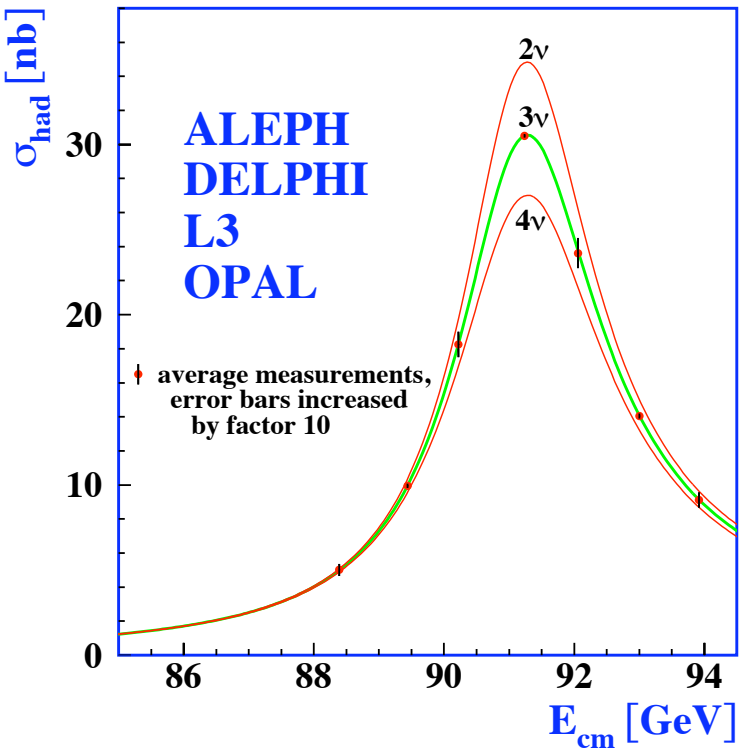

Figure 3: The curves indicate the hadronic cross-sections of different neutrino species, two, three and four, from predictions; the red dots are the measurements from ALEPH, DELPHI, etc.

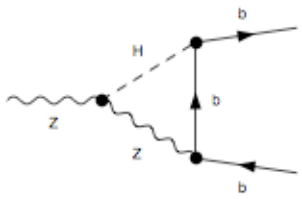

Figure 4: A one-loop example of the process $Z \to b\bar{b}$.

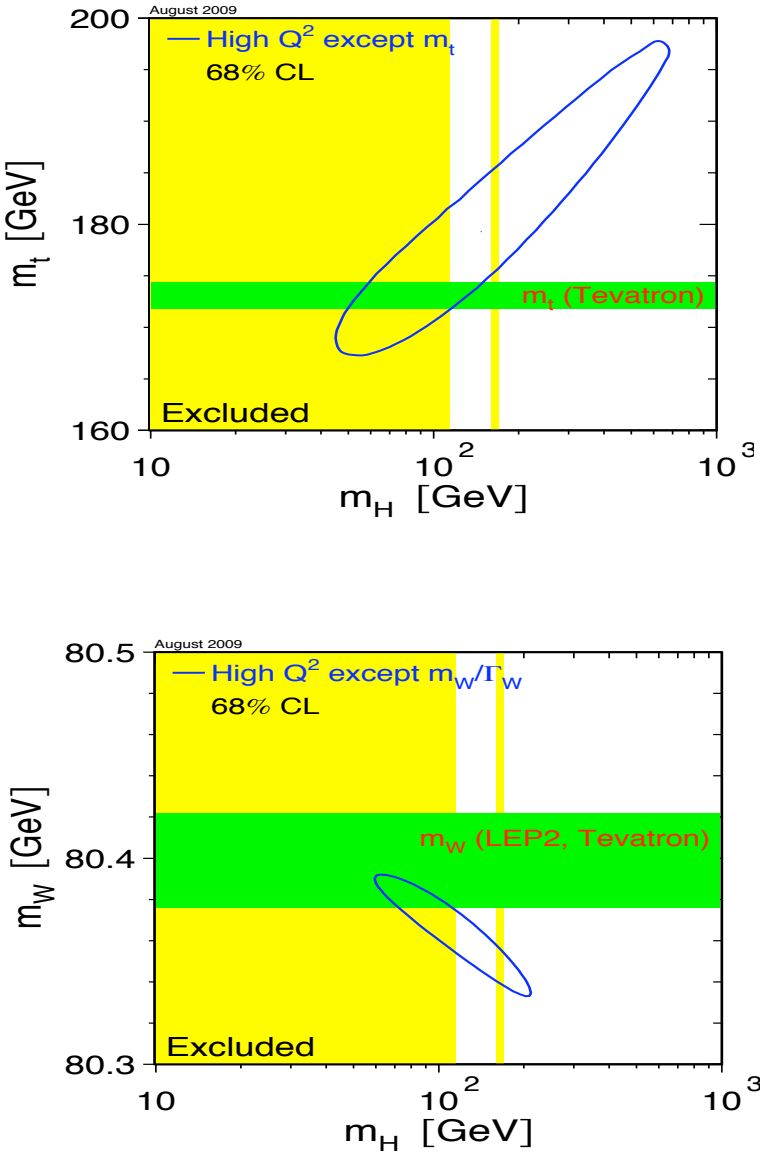

Figure 5: Contour curves of 68% propability in (a) the (m_t, m_H) plane and (b) the (m_W, m_H) plane, based on the measurements except the direct measurement of m_t and the direct measurements of m_H and $\Gamma_{\rm W}$ [1]. The horizontal bands of width ± 1 standard deviation show the corresponding observables of the direct measurements. The vertical yellow band shows the 95% confidence level exclusion limit on m_H of 114.4 GeV.

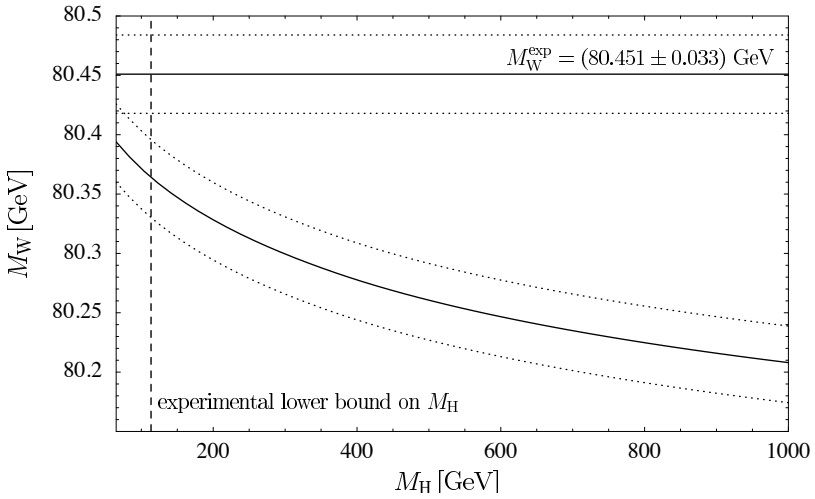

Figure 6: The prediction of M_W with up to two-loop fermionic corrections as compared to the experimental value [3], $M_W^{exp} = 80.419 \pm 0.038$ GeV [16] and the experimental 95% C.L. lower bound on the Higg-boson mass, $M_H = 107.9$ GeV [17].

3.0 ON-SHELL RENORMALIZATION

In the previous chapter, we have discussed the Standard Model which describes the electroweak interactions. However, more work is needed to deal with the difficulties that the SM has brought into, such as the divergences of the loop calculations in the perturbation. In the theory of renormalization, there are several different schemes for various circumstances, such as the $\overline{MS}$ renormalization scheme, which is convenient when no physically motivated prescription exists. For the one-loop level, the renormalization procedure has been worked completely [18, 19]. In our calculations, the on-shell renormalization scheme up to the NNLO [20] is adopted and will be briefly described in this chapter.

In the SM, the quantities that appear in the Lagrangian density are not physical observables, such as the masses, couplings and the fields, which referred to bare ones without dependence of energy scales. The physical quantity, such as the electron mass, in the on-shell renormalization scheme, is defined as the pole of the electron propagator; the electron charge is fixed at the vertex of the interaction between the electrons and the photons at certain energy scale. The above requirements are reached through the on-shell renormalization conditions with the counterterms which are derived from the bare Lagrangian.

In the following section, the renormalization constants and bare Lagrangian are defined in a specific gauge, and the counterterms for the self-energies and the vertices up to two-loop level are derived. In the second section, the renormalization conditions are discussed. Even though the on-shell renormalization is well understood at one-loop level, there are some different features that have to be taken into account for the NNLO. First, the products of one-loop counterterms can not be ignored, since their presence is shown in the two-loop level. Secondly, the interactions in the ghost sector have to be included in the calculation of the process $Z \to b\bar{b}$. At one-loop level, the contribution from the ghost can be neglected since there it does not directly interact with fermions. However, the lowest order that the ghost shows its contribution through interacting with vector bosons in one of the sub-loop is the NNLO. In the last section, the renormalization of the weak mixing angle and the charge are depicted briefly.

3.1 RENORMALIZATION CONSTANTS AND COUNTERTERMS

In order to absorb the UV divergences from the loop integrations, various renormalization constants are separated from the bare Lagrangian [18, 19, 20]. The renormalization transformations are listed

as below.

$$
\begin{array}{ll}
e_0 = Z_e e, & \\
s_{W0} = s_W + \delta s_W, & \\
M^2_{W0} = M^2_W + \delta M^2_W, & M^2_{Z0} = M^2_Z + \delta M^2_Z, \\
M^2_{H0} = M^2_H + \delta M^2_H, & m_{f0} = m_f + \delta m_f, \\
W^{\pm}_0 = (Z^W)^{\frac{1}{2}} W^{\pm}, & Z_0 = (Z^{ZZ})^{\frac{1}{2}} Z + \frac{1}{2}\delta Z^{Z\gamma} A, \\
 & A_0 = (Z^{\gamma\gamma})^{\frac{1}{2}} A + \frac{1}{2}\delta Z^{\gamma Z} Z, \\
\phi^{\pm}_0 = (Z_\phi)^{\frac{1}{2}} \phi^{\pm}, & \chi_0 = (Z_\chi)^{\frac{1}{2}} \chi \\
H_0 = (Z^H)^{\frac{1}{2}} H & f^L_0 = (Z^{fL})^{\frac{1}{2}} f^L, \\
 & f^L_0 = (Z^{fL})^{\frac{1}{2}} f^L.
\end{array}
\tag{3.1}
$$

Of those with an index 0, they are the bare quantities, which contain physical observables, such as mass M_X, and the corresponding renormalization constants δM_X, namely $M_{X0} = M_X + \delta M_X$. For the fields, the renormalization constants can be written as $Z_X = 1 + \delta Z_X$. And s_W is the sine of the weak mixing angle, $\sin\theta_W$.

The part of the bare Lagrangian of the gauge bosons and the unphysical Higgs fields with the R_ξ gauge in (2.9) reads as follows

$$
\begin{aligned}
L \;=\; & -\frac{1}{4}(F^+_{0\mu\nu}F^{-\mu\nu}_0 + F^-_{0\mu\nu}F^{+\mu\nu}_0) + \frac{1}{2}M^2_{W0}(W^+_{0\mu}W^{-\mu}_0 + W^-_{0\mu}W^{+\mu}_0) \\
& -\frac{1}{2\xi^W_1}\left((\partial_\mu W^{+\mu}_0)(\partial_\nu W^{-\nu}_0) + (\partial_\mu W^{-\mu}_0)(\partial_\nu W^{+\nu}_0)\right) \\
& -\frac{1}{4}F^Z_{0\mu\nu}F^{Z\mu\nu}_0 + \frac{1}{2}M^2_{Z0}Z_{0\mu}Z^\mu_0 - \frac{1}{2\xi^Z_1}\partial_\mu Z^\mu_0 \partial_\nu Z^\nu_0 \\
& -\frac{1}{4}F^A_{0\mu\nu}F^{A\mu\nu}_0 - \frac{1}{2\xi^A_1}\partial_\mu A^\mu_0 \partial_\nu A^\nu_0 \\
& -\frac{1}{2}\left((\partial_\mu\phi^+_0)(\partial^\mu\phi^-_0) + (\partial_\mu\phi^-_0)(\partial^\mu\phi^+_0)\right) - \frac{\xi^W_2}{2}M^2_{W0}(\phi^+_0\phi^-_0 + \phi^-_0\phi^+_0) \\
& -\frac{1}{2}(\partial_\mu\chi_0)(\partial^\mu\chi_0) - \frac{\xi^Z_2}{2}M^2_{Z0}\chi^2_0 \\
& +\frac{(\xi^Z_2)^{\frac{1}{2}}}{2(\xi^Z_1)^{\frac{1}{2}}}M_{Z0}(\partial_\mu Z^\mu_0)\chi_0 \\
& -\frac{i\xi^{W\,1/2}_2}{2\xi^{W\,1/2}_1}M_{W0}\left((\partial_\mu W^{+\mu}_0)\phi^-_0 + \phi^-_0(\partial_\mu W^{+\mu}_0) - (\partial_\mu W^{-\mu}_0)\phi^+_0 - \phi^+_0(\partial_\mu W^{-\mu}_0)\right),
\end{aligned}
$$

where

$$
\begin{aligned}
F^\pm_{\mu\nu} &= \partial_\mu W^\pm_\nu - \partial_\nu W^\pm_\mu, \\
F^Z_{\mu\nu} &= \partial_\mu Z_\nu - \partial_\nu Z_\mu, \\
F^A_{\mu\nu} &= \partial_\mu A_\nu - \partial_\nu A_\mu,
\end{aligned}
$$

and the gauge parameters of ξ's are defined in (2.9). With the definitions of renormalization constants (3.1), separate the counterterms into first and second orders, such as

$$
\begin{aligned}
\delta M^2_X &= \delta M^2_{X(1)} + \delta M^2_{X(2)}, \\
\delta Z^X &= \delta Z^X_{(1)} + \delta Z^X_{(2)}.
\end{aligned}
$$

Thus the Feynman rules derived from those counterterms can be obtained as follows. For self-energies of gauge bosons,

$$
\begin{aligned}
W^+W^-, \text{oneloop} &: -ig_{\mu\nu}\left[\delta Z^W_{(1)}(k^2-M_W^2)-\delta M^2_{W(1)}\right]+ik_\mu k_\nu \delta Z^W_{(1)},\\
\text{twoloop} &: -ig_{\mu\nu}\left[\delta Z^W_{(2)}(k^2-M_W^2)-\delta M^2_{W(2)}-\delta Z^W_{(1)}\delta M^2_{W(1)}\right]\\
&\quad +ik_\mu k_\nu \delta Z^W_{(2)}\\
Z^+Z^-, \text{oneloop} &: -ig_{\mu\nu}\left[\delta Z^{ZZ}_{(1)}(k^2-M_Z^2)-\delta M^2_{Z(1)}\right]+ik_\mu k_\nu \delta Z^{ZZ}_{(1)},\\
\text{twoloop} &: -ig_{\mu\nu}\left[\left(\delta Z^{ZZ}_{(2)}+\frac{1}{4}(\delta Z^{\gamma Z}_{(1)})^2\right)k^2-\delta Z^{ZZ}_{(2)}M_Z^2-\delta M^2_{Z(2)}\right.\\
&\quad \left.-\delta Z^{ZZ}_{(1)}\delta M^2_{Z(1)}\right]+ik_\mu k_\nu\left(\delta Z^{ZZ}_{(2)}+\frac{1}{4}(\delta Z^{\gamma Z}_{(1)})^2\right),\\
AA, \quad \text{oneloop} &: -ig_{\mu\nu}\delta Z^{\gamma\gamma}_{(1)}k^2+ik_\mu k_\nu \delta Z^{\gamma\gamma}_{(1)},\\
\text{twoloop} &: -ig_{\mu\nu}\left[\left(\delta Z^{\gamma\gamma}_{(2)}+\frac{1}{4}(\delta Z^{Z\gamma}_{(1)})^2\right)k^2-\frac{1}{4}(\delta Z^{Z\gamma}_{(1)})^2M_Z^2\right]\\
&\quad +ik_\mu k_\nu\left(\delta Z^{\gamma\gamma}_{(2)}+\frac{1}{4}(\delta Z^{Z\gamma}_{(1)})^2\right),\\
AZ, \quad \text{oneloop} &: -ig_{\mu\nu}\left[\frac{1}{2}(\delta Z^{Z\gamma}_{(1)}+\delta Z^{\gamma Z}_{(1)})k^2-\frac{1}{2}M_Z^2\delta Z^{Z\gamma}_{(1)}\right]\\
&\quad +\frac{i}{2}k_\mu k_\nu\left(\delta Z^{Z\gamma}_{(1)}+\delta Z^{\gamma Z}_{(1)}\right),
\end{aligned}
$$

$$
\begin{aligned}
\text{twoloop} &: -ig_{\mu\nu}\left[\frac{1}{2}\left(\delta Z^{Z\gamma}_{(2)}+\delta Z^{\gamma Z}_{(2)}+\frac{1}{2}\delta Z^{Z\gamma}_{(1)}\delta Z^{ZZ}_{(1)}+\frac{1}{2}\delta Z^{\gamma Z}_{(1)}\delta Z^{\gamma\gamma}_{(1)}\right)k^2\right.\\
&\quad \left.-\frac{1}{2}M_Z^2\delta Z^{Z\gamma}_{(2)}-\frac{1}{4}M_Z^2\delta Z^{ZZ}_{(1)}\delta Z^{Z\gamma}_{(1)}-\frac{1}{2}\delta M_Z^2\delta Z^{Z\gamma}_{(1)}\right]\\
&\quad +\frac{i}{2}k_\mu k_\nu\left(\delta Z^{Z\gamma}_{(2)}+\delta Z^{\gamma Z}_{(2)}+\frac{1}{2}\delta Z^{Z\gamma}_{(1)}\delta Z^{ZZ}_{(1)}+\frac{1}{2}\delta Z^{\gamma Z}_{(1)}\delta Z^{\gamma\gamma}_{(1)}\right). \qquad (3.2)
\end{aligned}
$$

For the counterterms of self-energies of unphysical parts of the Higgs sector, only one-loop levels are relevant with our calculations of $Z\to b\bar{b}$. The corresponding Feynman rules are

$$
\begin{aligned}
\chi\chi &: i\left[\delta Z^\chi_{(1)}+\frac{e\delta t}{2s_W M_W}\right],\\
\phi^+\phi^- &: i\left[\delta Z^\phi_{(1)}k^2+\frac{e\delta t}{2s_W M_W}\right],\\
W^\pm\phi^\mp &: \pm ik_\mu\frac{M_W}{2}\left[\delta Z^W_{(1)}+\delta Z^\phi_{(1)}+\frac{\delta M_W^2}{M_W^2}\right],\\
Z\chi &: \pm -k_\mu\frac{M_Z}{2}\left[\delta Z^{ZZ}_{(1)}+\delta Z^\chi_{(1)}+\frac{\delta M_Z^2}{M_Z^2}\right],\\
A\chi &: -k_\mu M_Z\frac{\delta Z^{Z\gamma}}{2}.
\end{aligned}
$$

As for the fermionic sector, the bare Lagrangian reads for one lepton generation, l, ν, and one quark generation, u, d,

$$\begin{aligned}\mathcal{L}^{\text{fermion}} &= i\bar{l}_0^L \not{\partial} l_0^L + i\bar{l_0}^R \not{\partial} l_0^R + i\bar{\nu}_0^L \not{\partial} \nu_0^L - \bar{l}_0^L m_{l0} l_0^R - \bar{l}_0^R m_{l0} l_0^L \\ &\quad + i\bar{u}_0^L \not{\partial} u_0^L + i\bar{u}_0^R \not{\partial} u_0^R + i\bar{d}_0^L \not{\partial} d_0^L + i\bar{d}_0^R \not{\partial} d_0^R \\ &\quad - \bar{u}_0^L m_{u0} u_0^R - \bar{d}_0^L m_{d0} d_0^R - \bar{u}_0^R m_{u0} u_0^L - \bar{d}_0^R m_{d0} d_0^L.\end{aligned}$$

Plugging the corresponding renormalization constants in (3.1), the resulting Feynman rules for counterterms are

$$\begin{aligned}l\bar{l},\ \text{oneloop} &: i\left[\delta Z_{(1)}^{l,R} \not{p}\omega_+ + \delta Z_{(1)}^{l,L} \not{p}\omega_- - \frac{m_l}{2}\delta Z_{(1)}^{l,R} - \frac{m_l}{2}\delta Z_{(1)}^{l,L} - \delta m_{l(1)}\right], \\ \text{twoloop} &: i\left[\delta Z_{(2)}^{l,R} \not{p}\omega_+ + \delta Z_{(2)}^{l,L} \not{p}\omega_- - \frac{m_l}{2}\delta Z_{(2)}^{l,R} - \frac{m_l}{2}\delta Z_{(2)}^{l,L} - \delta m_{l(2)}\right. \\ &\quad \left. + \delta m_{l(1)}\frac{\delta Z_{(1)}^{l,R}}{2} + \delta m_{l(1)}\frac{\delta Z_{(1)}^{l,L}}{2} + \frac{m_l}{8}(\delta Z_{(1)}^{l,R} - \delta Z_{(1)}^{l,L})^2\right], \\ \nu\bar{\nu},\ \text{oneloop} &: i\delta Z_{(1)}^{\nu,L} \not{p}\omega_-, \\ \text{twoloop} &: i\delta Z_{(2)}^{\nu,L} \not{p}\omega_-, \\ q\bar{q},\ \text{oneloop} &: i\left[\delta Z_{(1)}^{q,R} \not{p}\omega_+ + \delta Z_{(1)}^{q,L} \not{p}\omega_- - \frac{m_q}{2}\delta Z_{(1)}^{q,R} - \frac{m_q}{2}\delta Z_{(1)}^{q,L} - \delta m_{q(1)}\right], \\ \text{twoloop} &: i\left[\delta Z_{(2)}^{q,R} \not{p}\omega_+ + \delta Z_{(2)}^{q,L} \not{p}\omega_- - \frac{m_q}{2}\delta Z_{(2)}^{q,R} - \frac{m_q}{2}\delta Z_{(2)}^{q,L} - \delta m_{q(2)}\right. \\ &\quad \left. + \delta m_{q(1)}\frac{\delta Z_{(1)}^{q,R}}{2} + \delta m_{q(1)}\frac{\delta Z_{(1)}^{q,L}}{2} + \frac{m_q}{8}(\delta Z_{(1)}^{q,R} - \delta Z_{(1)}^{q,L})^2\right],\end{aligned}$$

where q could be up-type quark, u, or down-type quark, d.

For the calculations of the NNLO, the two-loop counterterms of the interaction must be incorporated. The Lagrangian related to the process, $Z \to b\bar{b}$, reads

$$\mathcal{L}_{Zb\bar{b}} = e_0 \bar{b}_0 Z_0 (g_0^- \omega_- + g_0^+ \omega_+) b_0,$$

where $g_0^- = \frac{-\frac{1}{2}+\frac{1}{3}s_{W0}^2}{s_{W0}c_{W0}}$ and $g_0^+ = \frac{s_{W0}}{3c_{W0}}$. We can denote the Lagrangian in terms of the renormalized quantities as

$$\mathcal{L}_{Zb\bar{b}} = e\bar{b} Z (C^- \omega_- + C^+ \omega_+) b,$$

where $C = 1 + \delta C_{(1)} + \delta C_{(2)}$ containing the countertems of higher orders. The counterterms of the one-loop level can be obtained as

$$\begin{aligned}\delta C_{(1)}^+ &= g_{(0)}^+ \left(\frac{\delta g_{(1)}^+}{g_{(0)}^+} + \delta Z_{e(1)} + \frac{1}{2}\delta Z_{(1)}^{ZZ} + \frac{1}{2}\delta Z_{(1)}^{bR} + \frac{1}{2}Z_{(1)}^{bR\dagger}\right) + \frac{1}{6}\delta Z_{(1)}^{\gamma Z}, \\ \delta C_{(1)}^- &= g_{(0)}^- \left(\frac{\delta g_{(1)}^-}{g_{(0)}^-} + \delta Z_{e(1)} + \frac{1}{2}\delta Z_{(1)}^{ZZ} + \frac{1}{2}\delta Z_{(1)}^{bL} + \frac{1}{2}Z_{(1)}^{bL\dagger}\right) + \frac{1}{6}\delta Z_{(1)}^{\gamma Z}.\end{aligned}$$

For the two-loop level, there are products of one-loop renormalization constants that have to be included, Thus we have

$$
\begin{aligned}
\delta C^{+}_{(2)} &= g^{+}_{(0)}\left[\frac{\delta g^{+}_{(2)}}{g^{+}_{(0)}} + \delta Z_{e(2)} + \frac{1}{2}\delta Z^{ZZ}_{(2)} + \frac{1}{2}\delta Z^{bR}_{(2)} + \frac{1}{2}Z^{bR\dagger}_{(2)}\right.\\
&\quad -\frac{1}{8}(\delta Z^{ZZ}_{(1)})^2 - \frac{1}{8}(\delta Z^{bR}_{(1)})^2 - \frac{1}{8}(\delta Z^{bR\dagger}_{(1)})^2\\
&\quad +\delta Z_{e(1)}\left(\frac{\delta g^{+}_{(1)}}{g^{+}_{(0)}} + \frac{1}{2}\delta Z^{ZZ}_{(1)} + \frac{1}{2}\delta Z^{bR}_{(1)} + \frac{1}{2}Z^{bR\dagger}_{(1)}\right)\\
&\quad +\frac{\delta g^{+}_{(1)}}{g^{+}_{(0)}}\frac{1}{2}\left(\delta Z^{ZZ}_{(1)} + \delta Z^{bR}_{(1)} + Z^{bR\dagger}_{(1)}\right)\\
&\quad \left.+\frac{1}{4}\left(\delta Z^{ZZ}_{(1)}\delta Z^{bR}_{(1)} + \delta Z^{ZZ}_{(1)}Z^{bR\dagger}_{(1)} + \delta Z^{bR}_{(1)}Z^{bR\dagger}_{(1)}\right)\right] + \frac{1}{6}\delta Z^{\gamma Z}_{(2)},\\
\delta C^{-}_{(2)} &= g^{-}_{(0)}\left[\frac{\delta g^{-}_{(2)}}{g^{-}_{(0)}} + \delta Z_{e(2)} + \frac{1}{2}\delta Z^{ZZ}_{(2)} + \frac{1}{2}\delta Z^{bL}_{(2)} + \frac{1}{2}Z^{bL\dagger}_{(2)}\right.\\
&\quad -\frac{1}{8}(\delta Z^{ZZ}_{(1)})^2 - \frac{1}{8}(\delta Z^{bL}_{(1)})^2 - \frac{1}{8}(\delta Z^{bL\dagger}_{(1)})^2\\
&\quad +\delta Z_{e(1)}\left(\frac{\delta g^{-}_{(1)}}{g^{-}_{(0)}} + \frac{1}{2}\delta Z^{ZZ}_{(1)} + \frac{1}{2}\delta Z^{bL}_{(1)} + \frac{1}{2}Z^{bL\dagger}_{(1)}\right)\\
&\quad +\frac{\delta g^{-}_{(1)}}{g^{-}_{(0)}}\frac{1}{2}\left(\delta Z^{ZZ}_{(1)} + \delta Z^{bL}_{(1)} + Z^{bL\dagger}_{(1)}\right)\\
&\quad \left.+\frac{1}{4}\left(\delta Z^{ZZ}_{(1)}\delta Z^{bL}_{(1)} + \delta Z^{ZZ}_{(1)}Z^{bL\dagger}_{(1)} + \delta Z^{bL}_{(1)}Z^{bL\dagger}_{(1)}\right)\right] + \frac{1}{6}\delta Z^{\gamma Z}_{(2)},
\end{aligned}
$$

where $\delta g^{+}_{(1)} = \frac{\delta s_{W(1)}}{3c^3_W}$, $\delta g^{-}_{(1)} = -\frac{s^2_W - c^2_W}{2s^2_W c_W}\delta s_{W(1)} + \delta g^{+}_{(1)}$ and those of the second order are in the same form.

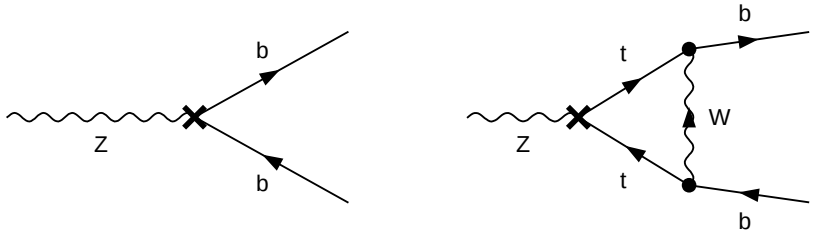

(a) (b)

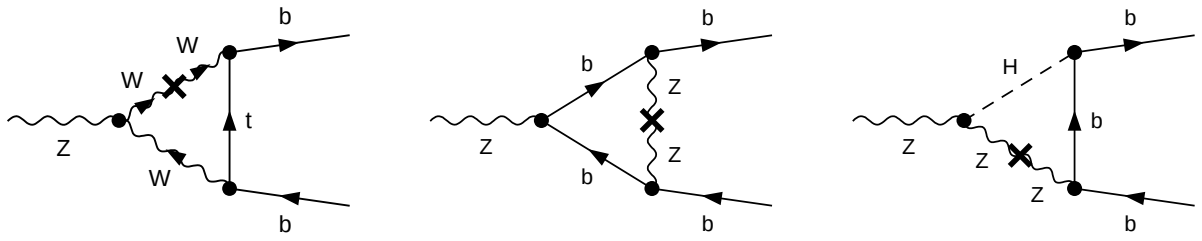

(c) (d) (e)

Figure 7: Some examples of two-loop counterterms which contribute to the weak mixing angle, $\sin\theta_W^{b\bar{b}}$.

3.2 ON-SHELL RENORMALIZATION CONDITIONS

With the definitions of the renormalization constants and counterterms, one needs further to specify the renormalization conditions to fix the physical quantities, such as the physical masses and coupling constants. Before getting this done, some of the renormalized quantities have to be discussed. The renormalized one-particle irreducible two-point functions are defined as follows

$$\begin{aligned}
\hat{\Gamma}^W_{\mu\nu}(k) &= -ig_{\mu\nu}(k^2 - M_W^2) - i\left(g_{\mu\nu} - \frac{k_\mu k_\nu}{k^2}\right)\hat{\Sigma}^W_T(k^2) - i\frac{k^\mu k^\nu}{k^2}\hat{\Sigma}^W_L(k^2) \\
\hat{\Gamma}^{ab}_{\mu\nu}(k) &= -ig_{\mu\nu}(k^2 - M_a^2)\delta_{ab} - i\left(g_{\mu\nu} - \frac{k_\mu k_\nu}{k^2}\right)\hat{\Sigma}^{ab}_T(k^2) - i\frac{k^\mu k^\nu}{k^2}\hat{\Sigma}^{ab}_L(k^2),
\end{aligned} \tag{3.3}$$

where $a = A, Z$, $M_A = 0$. The hat means the renormalized quantities; $\hat{\Sigma}^{ab}_T(k^2)$ denotes the transverse part of the renormalized self-energy at momentum k^2 and $\hat{\Sigma}^{ab}_L(k^2)$ is the longitudinal part. Similarly, for those of Higgs particles and fermions

$$\begin{aligned}
\hat{\Gamma}^H(k) &= i(k^2 - M_H^2) + i\hat{\Sigma}^H(k^2), \\
\hat{\Gamma}^f_{ij}(k) &= i\delta_{ij}(\not{p} - m_{f,i}) + i\Big[\not{p}\omega_-\hat{\Sigma}^{f,L}_{ij}(p^2) + \not{p}\omega_+\hat{\Sigma}^{f,R}_{ij}(p^2) \\
&\qquad + (m_{f,i}\omega_- + m_{f,j}\omega_+)\hat{\Sigma}^{f,S}_{i,j}(p^2)\Big].
\end{aligned} \tag{3.4}$$

The propagators of the corresponding particles can be obtained from the inverse of the two-point functions listed above. In order to fix to the renormalized masses, they are defined as the real parts of the poles of the propagators to be the physical masses, which are the so called on-shell

renormalization conditions. As for the unstable particles, the complex pole of the S matrix, $\mathcal{M}^2$, is different from the physical mass at the two-loop level, namely

$$\mathcal{M}_X^2 = \overline{M}_X^2 - i\overline{M}_X\,\Delta^X, \tag{3.5}$$

where $\overline{M}_X$ and Δ^X refer to the corresponding mass and the width of the unstable particle. The renormalization conditions which are defined by the propagators of the particles read

$$\begin{aligned}
(D_T^W)^{-1}(\mathcal{M}_W^2) = 0, \qquad & \Re\left\{\frac{\partial}{\partial k^2}(D_T^W)^{-1}(k^2)\Big|_{k^2=\mathcal{M}_W^2}\right\} = i,\\
(D_T^{ZZ})^{-1}(\mathcal{M}_Z^2) = 0, \qquad & (D_T^{\gamma Z})^{-1}(\mathcal{M}_Z^2) = 0,\\
(D_T^{Z\gamma})^{-1}(0) = 0, \qquad & (D_T^{\gamma\gamma})^{-1}(0) = 0,\\
\Re\left\{\frac{\partial}{\partial k^2}(D_T^{ZZ})^{-1}(k^2)\Big|_{k^2=\mathcal{M}_Z^2}\right\} = i, \qquad & \Re\left\{\frac{\partial}{\partial k^2}(D_T^{\gamma\gamma})^{-1}(k^2)\Big|_{k^2=0}\right\} = i,\\
(D_T^H)^{-1}(\mathcal{M}_H^2) = 0, \qquad & \Re\left\{\frac{\partial}{\partial k^2}(D_T^H)^{-1}(k^2)\Big|_{k^2=\mathcal{M}_H^2}\right\} = i\\
(D_T^f)^{-1}(p)\Big|_{p^2=\mathcal{M}_f^2} = 0, \qquad & \Re\left\{\frac{\partial}{\partial \not{p}}(D_T^W)^{-1}(p)\Big|_{p^2=\mathcal{M}_f^2}\right\} = i,
\end{aligned} \tag{3.6}$$

where $D_T^X(k^2)$ denote transverse parts of the propagator of the vector or scalar particle, X, and $D^f(p)$ for that of fermion, f. The propagators are related to the renormalized one-particle irreducible two-point functions, (3.3) and (3.4), as follows,

$$\begin{aligned}
D_T^W(k^2) = -\left(\hat{\Gamma}_T^W(k^2)\right)^{-1} \quad , \qquad & D^H(k^2) = -\left(\hat{\Gamma}^H(k^2)\right)^{-1},\\
\begin{pmatrix} D_T^{ZZ} & D_T^{\gamma Z} \\ D_T^{Z\gamma} & D_T^{\gamma\gamma} \end{pmatrix} = -\begin{pmatrix} \hat{\Gamma}_T^{ZZ} & \hat{\Gamma}_T^{\gamma Z} \\ \hat{\Gamma}_T^{Z\gamma} & \hat{\Gamma}_T^{\gamma\gamma} \end{pmatrix}^{-1} \quad &= \quad \frac{-1}{\hat{\Gamma}_T^{ZZ}\hat{\Gamma}_T^{\gamma\gamma} - \hat{\Gamma}_T^{\gamma Z}\hat{\Gamma}_T^{Z\gamma}} \begin{pmatrix} \hat{\Gamma}_T^{\gamma\gamma} & -\hat{\Gamma}_T^{Z\gamma} \\ -\hat{\Gamma}_T^{\gamma Z} & \hat{\Gamma}_T^{ZZ}, \end{pmatrix},\\
D^f = -(\hat{\Gamma}^f)^{-1}.
\end{aligned}$$

With the renormalization conditions stated above, one is able to obtain the renormalization constants of masses and fields from $\hat{\Sigma} = \Sigma + \text{counterterms}$. At one loop level, there is no problem related to the complex poles, $\mathcal{M}^2$, due to the imaginary part being of one-loop order itself; we have

$$\begin{aligned}
\delta M_{W(1)} = \Re\{\Sigma_T^W(M_W^2)\}, \qquad & \delta Z_{(1)}^W = -\Re\{\Sigma_T^{W\prime}(M_W^2)\},\\
\delta M_{Z(1)} = \Re\{\Sigma_T^{ZZ}(M_Z^2)\}, \qquad & \delta Z_{(1)}^{ZZ} = -\Re\{\Sigma_T^{ZZ\prime}(M_Z^2)\},\\
\delta Z_{(1)}^{\gamma Z} = -2\Re\left\{\frac{\Sigma_T^{\gamma Z}(M_Z^2)}{M_Z^2}\right\}, \qquad & \delta Z_{(1)}^{\gamma Z} = 2\frac{\Sigma_T^{\gamma Z}(0)}{M_Z^2},\\
\delta Z_{(1)}^{\gamma\gamma} = -\Sigma_T^{\gamma\gamma\prime}(0), & \\
\delta M_{H(1)} = \Re\{\Sigma_T^H(M_H^2)\}, \qquad & \delta Z_{(1)}^H = -\Re\{\Sigma_T^{H\prime}(M_H^2)\},
\end{aligned} \tag{3.7}$$

$$
\begin{aligned}
\delta m_{f(1)} &= \frac{m_f}{2}\Re\left\{\Sigma^f_{L(1)}(m_f^2)+\Sigma^f_{R(1)}(m_f^2)+2\Sigma^f_{S(1)}(m_f^2)\right\},\\
\delta Z^{fL}_{(1)} &= -\Re\{\Sigma^f_{L(1)}(m_f^2)\}-m_f^2\Re\left\{\Sigma^{f\prime}_{L(1)}(m_f^2)+\Sigma^{f\prime}_{R(1)}(m_f^2)+2\Sigma^{f\prime}_{S(1)}(m_f^2)\right\},\\
\delta Z^{fR}_{(1)} &= -\Re\{\Sigma^f_{R(1)}(m_f^2)\}-m_f^2\Re\left\{\Sigma^{f\prime}_{L(1)}(m_f^2)+\Sigma^{f\prime}_{R(1)}(m_f^2)+2\Sigma^{f\prime}_{S(1)}(m_f^2)\right\}.
\end{aligned}
$$

For the next level, the imaginary part of the complex pole in (3.5) has to be taken into account. From the renormalization condition (3.6) of the $W^\pm$ boson, one has

$$
\hat{\Gamma}^W_T(\mathcal{M}^2_W) = -i\left[\mathcal{M}^2_W - M^2_W + \hat{\Sigma}^W_T(\mathcal{M}^2_W)\right] = 0.
$$

By taking the real and imaginary part of the above equation, including the counterterms of the Z boson propagator in (3.2) for the renormalized two-point function, the condition becomes

$$
\begin{aligned}
&\delta M^2_{W(2)} = \Re\{\Sigma^W_{T(2)}(M^2_W)\}+\Re\left\{\Sigma^{W\prime}_{T(1)}(M^2_W)\cdot\left(-iM_W\Delta^W_{(1)}(M^2_W)\right)\right\}-\delta Z^W_{(1)}\delta M^2_{W(1)},\\
&\Delta^W_{(1)}(M^2_W) = \frac{1}{M_W}\Im\{\Sigma^W_{T(1)}(M^2_W)\},
\end{aligned}
$$

thus we have for the two-loop renormalization condition for the mass of the $W^\pm$ boson

$$
\delta M^2_{W(2)} = \Re\{\Sigma^W_{T(2)}(M^2_W)\}-\Im\left\{\Sigma^{W\prime}_{T(1)}(M^2_W)\right\}\Im\left\{\Sigma^W_{T(1)}(M^2_W)\right\}-\delta Z^W_{(1)}\delta M^2_{W(1)}.
$$

When considering the Z boson propagator, the 2-point function related to the Z boson and photon, $\hat{\Sigma}^{\gamma Z}$ has to be included. Hence, we have

$$
(D^{ZZ}_T)^{-1}(\mathcal{M}^2_Z) = -i\left[\mathcal{M}^2_Z - M^2_Z + \hat{\Sigma}^{ZZ}_T(\mathcal{M}^2_Z) - \frac{\left(\hat{\Sigma}^{\gamma Z}_T(\mathcal{M}^2_Z)\right)^2}{\mathcal{M}^2_Z+\hat{\Sigma}^{\gamma\gamma}_T(\mathcal{M}^2_Z)}\right] = 0.
$$

The last term in the middle equation comes from a series of photons interacting with the ingoing and the outgoing Z bosons through one particle irreducible two-point functions, $\hat{\Sigma}^{\gamma Z}_T$ and $\hat{\Sigma}^{\gamma\gamma}_T$. Similarly, taking the real and imaginary parts of the above condition with the corresponding counterterm in (3.2),

$$
\begin{aligned}
\delta M^2_{Z(2)} &= \Re\{\Sigma^{ZZ}_{T(2)}(M^2_Z)\}+\Re\left\{\Sigma^{ZZ\prime}_{T(1)}(M^2_Z)\cdot\left(-iM_Z\Delta^Z_{(1)}(M^2_Z)\right)\right\}\\
&\quad -\delta Z^{ZZ}_{(1)}\delta M^2_{Z(1)}+\frac{M^2_Z}{4}(\delta Z^{\gamma Z}_{(1)})^2+\Re\left\{\frac{\left(\hat{\Sigma}^{\gamma Z}_{T(1)}(M^2_Z)\right)^2}{M^2_Z}\right\}, \qquad (3.8)\\
\Delta^Z_{(1)}(M^2_Z) &= \frac{1}{M_Z}\Im\{\Sigma^{ZZ}_{T(1)}(M^2_Z)\}. \qquad (3.9)
\end{aligned}
$$

The last term in (3.8) can be obtained from the on-shell scheme of (3.7), thus $\hat{\Sigma}^{\gamma Z}_{T(1)}(M_Z^2) = i\Im\{\Sigma^{\gamma Z}_{T(1)}(M_Z^2)\}$ and with (3.9) it ends up

$$\begin{aligned}\delta M^2_{Z(2)} &= \Re\{\Sigma^{ZZ}_{T(2)}(M_Z^2)\} - \Im\left\{\Sigma^{ZZ\prime}_{T(1)}(M_Z^2)\right\}\Im\left\{\Sigma^{ZZ}_{T(1)}(M_Z^2)\right\} \\ &\quad -\delta Z^{ZZ}_{(1)}\delta M^2_{Z(1)} + \frac{M_Z^2}{4}(\delta Z^{\gamma Z}_{(1)})^2 + \frac{\Im\left\{\Sigma^{\gamma Z}_{T(1)}(M_Z^2)\right\}^2}{M_Z^2}.\end{aligned}$$

For the Fermions at the two-loop level, the mass and the field renormalizations are

$$\begin{aligned}\delta m_{f(2)} &= \frac{m_f}{2}\Re\left\{\Sigma^f_{L(2)}(m_f^2) + \Sigma^f_{R(2)}(m_f^2) + 2\Sigma^f_{S(2)}(m_f^2)\right\} \\ &\quad +\frac{1}{4}\Re\left\{(\Sigma^f_{R(1)}(m_f^2) - \Sigma^f_{L(1)}(m_f^2))^2\right\} - \frac{\delta m_f}{2}\left(\Sigma^f_{R(1)}(m_f^2) + \Sigma^f_{L(1)}(m_f^2)\right), \\ \delta Z^{fL}_{(2)} &= -\Re\{\Sigma^f_{L(2)}(m_f^2)\} - m_f^2\Re\left\{\Sigma^{f\prime}_{L(2)}(m_f^2) + \Sigma^{f\prime}_{R(2)}(m_f^2) + 2\Sigma^{f\prime}_{S(2)}(m_f^2)\right\}, \\ \delta Z^{fR}_{(2)} &= -\Re\{\Sigma^f_{R(2)}(m_f^2)\} - m_f^2\Re\left\{\Sigma^{f\prime}_{L(2)}(m_f^2) + \Sigma^{f\prime}_{R(2)}(m_f^2) + 2\Sigma^{f\prime}_{S(2)}(m_f^2)\right\}.\end{aligned}$$

3.3 RENORMALIZATION OF THE WEAK MIXING ANGLE AND THE CHARGE

The weak mixing angle is defined from the masses of the gauge bosons, namely

$$\sin\theta_W \equiv s_W = \sqrt{\frac{M_Z^2 - M_W^2}{M_Z^2}},\ \cos\theta_W \equiv c_W = \frac{M_W}{M_Z},$$

and the same for the corresponding bare quantities. Since the bare masses are

$$\begin{aligned}M^2_{W0} &= M_W^2 + \delta M^2_{W(1)} + \delta M^2_{W(2)}, \\ M^2_{Z0} &= M_W^2 + \delta M^2_{Z(1)} + \delta M^2_{Z(2)},\end{aligned}$$

then it can be obtained that $s_{W0} = s_W + \delta s_{W(1)} + \delta s_{W(2)}$, where

$$\begin{aligned}\delta s_{W(1)} &= \frac{1}{2s_W M_Z^2}\left(\frac{M_W^2}{M_Z^2}\delta M^2_{Z(1)} - \delta M^2_{W(1)}\right), \\ \delta s_{W(2)} &= \frac{1}{2s_W M_Z^2}\left(\frac{M_W^2}{M_Z^2}\delta M^2_{Z(2)} - \delta M^2_{W(2)}\right)\end{aligned}$$

$$\begin{aligned}&-\frac{M_W^2(4M_Z^2 - 3M_W^2)}{8M_Z^8 s_W^3}(\delta M^2_{Z(1)})^2 - \frac{1}{8M_Z^4 s_W^3}(\delta M^2_{W(1)})^2 \\ &+\frac{2M_Z^2 - M_W^2}{4M_Z^6 s_W^3}\delta M^2_{Z(1)}\delta M^2_{W(1)}.\end{aligned}$$

In the next step, the on-shell conditions of the charge renormalization,

$$\hat{\Gamma}^{\gamma \bar{f}^{L,R} f^{L,R}}(0,-p,p)\Big|_{p^2=m_f^2} = -ieQ\gamma_\mu, \tag{3.10}$$

where Q is the charge quantum number of the fermion, has to be fulfilled in all orders of perturbation theory. For simplicity, we adopt the result from the Slavnov-Taylor identity [19],

$$\begin{aligned}
&\hat{\Gamma}^{\gamma \bar{f}^{L,R} f^{L,R}}(k_1^2=0, k_2^2=m_f^2, k_3^2=m_f^2) \\
&= -e_0 Q \left((Z^{\gamma\gamma})^{\frac{1}{2}} + \frac{s_{W0}}{c_{W0}} \frac{\delta Z^{Z\gamma}}{2} \right) \frac{\partial}{\partial k^\mu} \hat{\Gamma}^{\bar{f}^{L,R} f^{L,R}}(k)\Big|_{k^2=m_f^2},
\end{aligned} \tag{3.11}$$

where $f^{L,R}$ means the fermion could be either f^L or f^R for all of them. Besides, the renormalization conditions, (3.6), of fermion propagator state that

$$\frac{\partial}{\partial k^\mu} \hat{\Gamma}^{\bar{f}^{L,R} f^{L,R}}(k)\Big|_{k^2=m_f^2} = i\gamma_\mu.$$

When combined with (3.10) and (3.11), they give

$$-ieQ \;\; = \;\; -iZ_e Q \left((Z^{\gamma\gamma})^{\frac{1}{2}} + \frac{Z_{s_W}}{Z_{c_W}} \frac{s_W}{c_W} \frac{\delta Z^{Z\gamma}}{2} \right),$$

so that

$$Z_e \left((Z^{\gamma\gamma})^{\frac{1}{2}} + \frac{Z_{s_W}}{Z_{c_W}} \frac{s_W}{c_W} \frac{\delta Z^{Z\gamma}}{2} \right) = 1.$$

For the one-loop level, we obtain the condition for the charge renormalization

$$\delta Z_{e(1)} = -\frac{1}{2}\delta Z^{\gamma\gamma}_{(1)} - \frac{s_W}{c_W}\frac{1}{2}\delta Z^{Z\gamma}_{(1)},$$

with the result of two-loop level,

$$\delta Z_{e(2)} = -\frac{1}{2}\delta Z^{\gamma\gamma}_{(2)} - \frac{s_W}{c_W}\frac{1}{2}\delta Z^{Z\gamma}_{(2)} + (\delta Z^{Z\gamma}_{(1)})^2 + \frac{1}{8}(\delta Z^{\gamma\gamma}_{(1)})^2 - \frac{1}{2c_W^3}\delta Z^{Z\gamma}_{(1)}\delta s_{W(1)}.$$

4.0 NUMERICAL METHODS OF EVALUATING TWO-LOOP FEYNMAN INTEGRALS

The difficulty of the loop integration lies in the presence of the divergence. In addition, analytic treatments are not generally achievable for diverse processes; therefore there has been much effort beyond 1-loop made to develop numerical techniques to evaluate Feynman integrals, such as dispersion relation [21, 22, 5], expansion by regions [23, 24], as well as some supplementary techniques, like integration by part (IBP) [25]. For different methods, they have their own advantages and limitations. For instance, sector decomposition [26], an alternative method of computing a oop integral numerically, has the algorithm to isolate the poles; however, it obtains a large number of the integrals. In the case of the dispersion relation, no algorithm is known to extract singularities and is difficult to automatic the procedure for more complex diagrams. The motivation of this project is to extend and improve the previous works of [27] in algorithmic techniques of evaluating loop integrals with Mellin-Barnes representation. Like other numerical techniques, its advantage is that it has a general way to isolate the singularities, but what ends up in the representation are the complex multi-dimensional integrals. Our goal in this thesis is to improve the numerical integration methods for MB representation for high dimensions and with arbitrary masses.

This chapter is outlined as follows. In the next section, the derivation of Mellin-Barnes representation is briefly described, and the method to isolate the divergences will be discussed. Then the techniques of numerical integration, such as Gaussian Quadrature (GQ), Monte Carlo methods (MC) and an essential trick to reduce the dimension of the integration, are also presented in the second section. In the actual calculations, the results of the thesis are the outcome of the mixed uses of some of the numerical techniques mentioned in the first paragraph. Therefore, in the last section, some discussions of the other methods are presented in order to give some basic ideas of those approaches.

4.1 MELLIN-BARNES REPRESENTATION

The way that theorists deal with divergence is called regularization and renormalization. One of the methods to isolate the singularities is so-called dimensional regularization. It is convenient to apply the Feynman parametrization on the loop integrals. The formula is

$$\frac{1}{A_1 A_2 ... A_n} = \int_0^1 dx_1 dx_2 ... dx_n \delta(\sum x_i - 1) \frac{(n-1)!}{[x_1 A_1 + x_2 A_2 + ... + x_n A_n]^n}. \tag{4.1}$$

The next step is to integrate the loop momentum over d dimensions, instead of 4, then in the end d is replaced by $d = 4 - 2\varepsilon$. Typically, the loop momenta, k, are transformed to Euclidean space,

$k^0 \equiv ik_E$ and $\mathbf{k} \equiv \mathbf{k_E}$, namely the Wick rotation; an example of an integral in d dimension is

$$\int \frac{d^dk}{i(\pi)^{d/2}} \frac{1}{[k^2-\Delta]^n} = (-1)^n \int \frac{d^dk_E}{(\pi)^{d/2}} \frac{1}{[k_E^2+\Delta]^n} = (-1)^n \frac{\Gamma(n-\frac{d}{2})}{\Gamma(n)} \frac{1}{\Delta^{\frac{d}{2}-n}}.$$

By expansions of ε around zero, the singularities, including UV, infrared or collinear divergence, appear in terms of $\frac{1}{\varepsilon}$, $\frac{1}{\varepsilon^2}$, etc. The goal of renormalization is to remove UV divergent terms so that the physical quantities are left convergent.

In order to obtain MB representation, the above technique is applied to incorporate different propagators which associate with the same loop into a denominator then use the basic formula

$$\frac{1}{(X+Y)^\lambda} = \frac{1}{\Gamma(\lambda)} \frac{1}{2\pi i} \int_{c-i\infty}^{c+i\infty} dz \Gamma(\alpha+z)\Gamma(-z) \frac{Y^z}{X^{\lambda+z}}, \tag{4.2}$$

where c is a real constant chosen to make the contour of integration separate the poles of $\Gamma(-z)$ and $\Gamma(\alpha+z)$, i.e. $-\mathrm{Re}(\alpha) < c < 0$. Then the Feynman parameters are integrated out according to the formula

$$\int_0^1 \prod_{i=1}^n d\alpha_i \alpha_i^{a_i-1} \delta(1-\sum_{i=1}^n \alpha_i) = \frac{\Gamma(a_1)\cdots\Gamma(a_n)}{\Gamma(a_1+\cdots+a_n)}.$$

A simple and typical Mellin-Barnes integral, after applied the above formulas, is

$$-\frac{1}{2\pi i}(Q^2)^{-1-\varepsilon} \int_{-i\infty}^{+i\infty} dz \left(\frac{m^2}{Q^2}\right)^z \frac{\Gamma(1+z)\Gamma(1+\varepsilon+z)\Gamma(-\varepsilon-z)^2\Gamma(-z)}{\Gamma(1-2\varepsilon-z)}, \tag{4.3}$$

which is derived from the one-loop triangle diagram with one massive propagator as shown in Figure 4 with $m_H = M_Z = 0$, $m_b = m$ and $Q^2 = -(p_1-p_2)^2$ (p_1 and p_2 are outgoing momenta of b quarks). For the criteria of the contours to be satisfied, ε might not be able to be 0 in the complex plane. Hence, to extract the singularities for $\varepsilon \to 0$, an algorithmic technique, which is based on the Cauchy theorem, is needed [27]. The idea is that, when ε is gradually approaching zero, some of the poles might go across the contour from one side to the other, just like the red dots in Figure 8 (b). We may take (4.3) as an example, though it does not give any crossing pole itself. Assume the third gamma function is replaced with $\Gamma(-1-\varepsilon-z)$. As mentioned below (4.2), the allowed contour for the modified (4.3) could be chosen as $z = -0.5 + iy$. Then it turns out to give a constraint to ε for $\varepsilon < -0.5$. The poles for the gamma function are at $z = -1-\varepsilon$, $-\varepsilon$, $1-\varepsilon$, ... It is apparent that, as ε goes to zero, the first pole at $z = -1-\varepsilon$ crosses the contour of $z = -0.5 + iy$ to reach the point at $z = -1$. As we apply the dimensional regularization, which requires $\varepsilon \to 0$, the residues of the crossing poles have to be added back to the MB representations, and in effect these residues result in more integrals of lower dimensions.

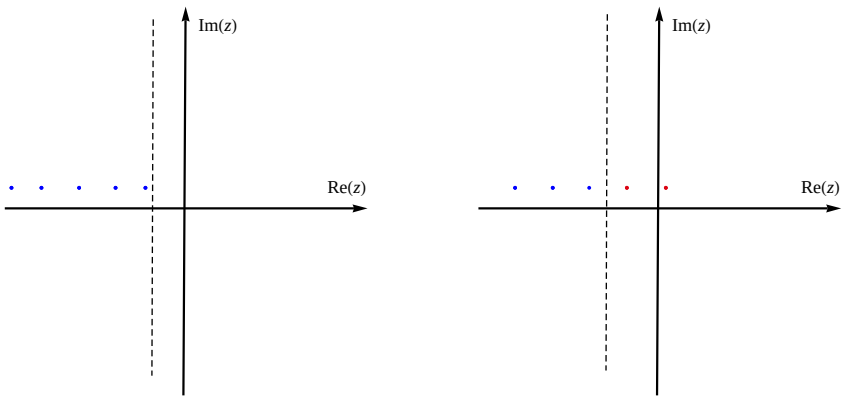

(a) (b)

Figure 8: The figure indicates the poles' movements when ε gradually moves toward zero as the contour of the integration also displaces to a different position, where (a) $\varepsilon \neq 0$ and (b) $\varepsilon \to 0$. The red dots represent the poles of the Gamma function, which come across the contour as ε goes to zero, and the blue dots do not.

4.2 INTEGRATION TECHNIQUES

4.2.1 Change of Variables

In some of the cases, the numerical integration does not converge well due to high dimensionality and a factor of the form, $e^{-i\pi z_k}$, which is usually present in the integrand. With respect to the variable z_k, the factor blows up exponentially in one of the imaginary directions and makes the oscillation of the integrand diminish at a very slow rate. In order to remedy this problem, we may use the example of the triangle diagram, (4.3). As $Q^2 < 0$, along the contour $z = c + iy$,

$$(Q^2)^{-z} \quad = \quad (-Q^2)^{-c-iy}(-1-i\epsilon)^{-c-iy} = (-Q^2)^{-c-iy}e^{i\pi c}e^{-\pi y}, \tag{4.4}$$

where c is a real constant and y is the variable along the imaginary axis of z. Even though the gamma functions approach zero quickly as the arguments drift away from the real axis, the factor $e^{-\pi y}$ makes the integrand decrease quite slowly as $y \to -\infty$. In the MB representation, the contours are chosen to go through the specific poles to separate one side of poles from the other, according to the criteria of the contours. Then they are allowed to be deformed, instead of just being parallel to the imaginary axis, as long as this criteria is satisfied. In order not to cross any poles from contour changing, a convenient way is to tilt all the contours by the same angle. A parameter is proposed to describe the change of contours, θ, for the contours go in the direction of $\theta + i$, hence the contour is changed to go along $z = c + (\theta + i)y$. The exponential factor becomes

$$(-Q^2)^{-z} = (-Q^2)^{-c-iy}e^{i\pi(c+\theta y)}e^{-(\pi+\theta\log(-Q^2))y}, \tag{4.5}$$

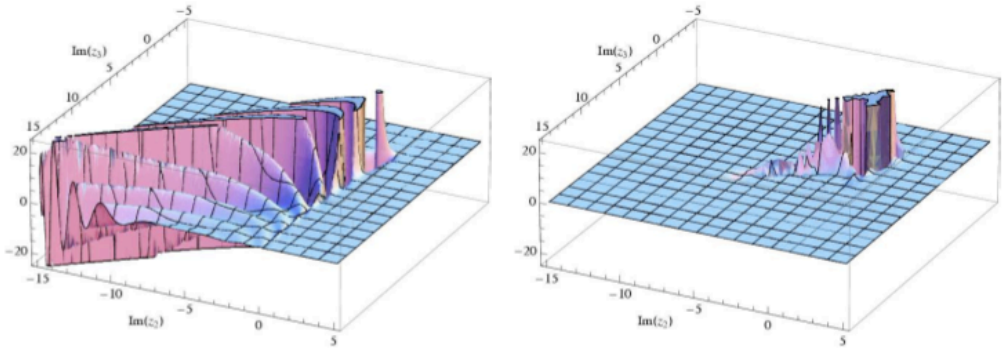

Figure 9: The real part of the integrand for the sunset diagram. For the left panel, the integration contours have been chosen as straight lines parallel to the imaginary axis, and the z_1 integration has already been carried out. For the right panel, the contours have been deformed by a rotation in the complex plane, corresponding to $\theta = 0.4$.

so that the problematic factor $e^{-\pi y}$ can be compensated by a suitable choice of θ. In Figure 9, the behavior of the integrand for the complex integral of the sunset diagram becomes more concentrated with less fluctuation due to the deformation of the contours, as shown in the right panel, so as to improve the efficiency of the numerical integration.

It is also helpful to change all the imaginary dimensions of the complex variables, $z_i = c_i + iy_i$, to hyper-spherical coordinate

$$\begin{aligned} y_1 &= r\cos\phi_1, \\ y_2 &= r\sin\phi_1\cos\phi_2, \\ \vdots &= \vdots \\ y_{n-1} &= r\sin\phi_1\cdots\sin\phi_{n-2}\cos\phi_{n-1}, \\ y_n &= r\sin\phi_1\cdots\sin\phi_{n-2}\sin\phi_{n-1}. \end{aligned}$$

The complex integration with the hyper-spherical coordinates is tested to be more effective as the integration region is shrunk from n dimensional infinite domain to a radial dimension times confined $(n-1)$ dimensional domain. However, for high dimensional cases, like 8 dimensions or higher, even with all of the above techniques it still takes a long time to reach an answer, say, with one percent accuracy. To resolve this issue, a method to reduce the dimension of the integral is proposed to solve the convergence problem.

4.2.2 Reduction of Integration Dimension

Even though the Monte Carlo is the most efficient for high dimension integration, it is still very difficult for an 8 or 9 dimensional integral to converge in a short period of time. Therefore, the idea to reduce the dimension of the integral could be a solution to make the numerical integration quicker. Below we propose several formulas which could be derived by the convolution theorem for Mellin transformation. We have worked on the derivation of additional formulas that could be useful for other integrals. The formulas, which are provided without proofs [28], have shown their powerfulness in the current work:

$$\frac{1}{2\pi i}\int_{\gamma-i\infty}^{\gamma+i\infty} du\Gamma(-u)\Gamma(\beta+u)t^u = \Gamma(\beta)\Gamma(1+t)^{-\beta} \qquad (4.6)$$
$$[0>\gamma>Re(1-\beta)],$$

$$\frac{1}{2\pi i}\int_{\gamma-i\infty}^{\gamma+i\infty} du\Gamma(\alpha-u)\Gamma(u)\Gamma(1-c+u)\Gamma(s-u)$$
$$= \frac{\Gamma(\alpha)\Gamma(\alpha-c+1)\Gamma(s)\Gamma(s-c+1)}{\Gamma(\alpha+s-c+1)} \qquad (4.7)$$
$$[Re(\alpha)-\gamma>0, \gamma>0, 1-Re(c)+\gamma>0, Re(s)-\gamma>0]$$

and

$$\frac{1}{2\pi i}\int_{\gamma-i\infty}^{\gamma+i\infty} \Gamma(-u)\Gamma(\beta+u)\Gamma(s+u)\Gamma(\alpha-s-u)m^{-s-u}du$$
$$= \frac{\Gamma(\alpha)\Gamma(\beta)\Gamma(\alpha+\beta-s)\Gamma(s)}{\Gamma(\alpha+\beta)}\,{}_2F_1(s,\alpha,\alpha+\beta,1-m). \qquad (4.8)$$
$$[0>\gamma>1-Re(\beta), 0>\gamma>1-Re(\alpha)]$$

Without these formulae the MB representation of the 5-propagator self-energy Feynman diagram in Figure 10, gives a 10-dim integral; however, with successive applications of these the dimension of the integral is reduced to 6. In general, with one dimension less, the convergence of the integration can be up to 20 times faster so that it would be the best if the dimension of integration is decreased as many as possible with proper contours chosen.

4.3 NUMERICAL INTEGRATION METHODS

Many numerical integration techniques are developed over centuries, like Simpson's rule, trapezoidal rule, etc. Here we present Gaussian quadrature, which is one of the most efficient integration methods, and the Monte Carlo method, which excels in high dimension integrations.

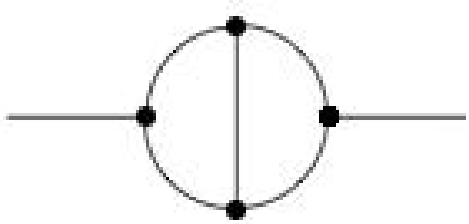

Figure 10: A 5-propagator self-energy Feynman diagram generates a 10-dim complex integral after being transformed into Mellin-Barnes representation.

4.3.1 Gaussian Quadrature

The main idea of Gaussian quadrature is to approximate an integral by a sum of the product of its functional values at specific abscissas within the interval $[a, b]$ and some weighting coefficients, such that

$$\int_a^b w(x)f(x)dx \approx \sum_k^n w_k f(x_k), \tag{4.9}$$

where $w(x)$ is the weight function and w_k is the weighting values corresponding to different points along x axis. $w(x)$ is used to define the inner product of functions and a set of orthonormal polynomials, $p_0(x)$, $p_1(x)$, ... ,i.e.

$$< p_m, p_n >= \int_a^b w(x)p_m(x)p_n(x)dx = \delta_{mn},$$

and abscissas are assigned to be the zeros of the polynomial $p_n(x)$. There are a few ways to obtain the weights, w_k; one example is to solve the set of the equations,

$$\begin{cases} \sum_k^n w_k p_0(x_k) = \int_a^b w(x)p_0(x)dx, \\ \sum_k^n w_k p_j(x_k) = 0, \qquad\qquad (j = 1, 2, ... n). \end{cases}$$

The reason that the second line equals to zero is because $p_0(x)$ is a constant and the rest of the polynomials, $p_j(x)$ (for $j \neq 0$) are orthogonal to it. There are various options for the choices of the

weight function, such as e^{-x}, the so called Gauss-Laguerre quadrature, for the interval $(0, \infty)$, and its weights are given by

$$w_k = \frac{x_k}{(n+1)^2 (L_{n+1}(x_k))^2},$$

where x_k is the k-th root of the Laguerre polynomial, $L_n(x)$.

The error, E_n, of the Gaussian Quadrature is given by

$$E_n(f) = \frac{(b-a)^{2n+1}(n!)^4}{(2n+1)[(2n)!]^3} f^{(2n)}(\xi), \quad -1 < \xi < 1.$$

Hence, as long as the function is well behaved, it can be seen that for $n = 5$ for the interval $[-1, 1]$, the error is only about 10^{-9} times its tenth derivative.

4.3.2 Monte Carlo Method

The Monte Carlo (MC) method is widely exploited for approximating the high dimensional integrations due to its power-law scaling of integration time. For instance, if we need to compute the integral

$$I = \int_a^b f(x)dx,$$

it can be estimated by sampling n points within the interval $[a, b]$ of x. Then we can expect the average of $f(x_i)$ for $i = \{1, 2, ..., n\}$ approaches the true value of I as $n \to \infty$ so we have

$$\int_a^b f(x)dx \approx \frac{b-a}{n}[f(x_1) + ... + f(x_n)].$$

In practice, some modifications are applied on MC method, like Vegas MC [29], which samples points according to the probability distribution function $|f|$ such that the points selected are concentrated in the region that makes the largest contribution to the integral.

4.4 OTHER NUMERICAL METHODS

In the previous sections, the Mellin-Barnes representation of the Feynman integrals is introduced, and its advantage is its generality for diverse topologies of the diagrams and various masses of the propagators. However, the drawback is the high dimensional complex integrals that appear in the representation, and it may result in the slow convergence of the numerical error or even divergence. Though many numerical methods have been presented and some new ones have been developed in this chapter, the dimension of the complex integral is still the main limitation of this method. Here some of the other useful approaches for computation of Feynman integrals are presented in brief, though each of them has its own benefits and limitations.

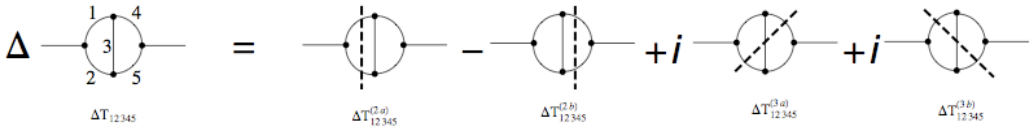

Figure 11: According to Cutkosky's rules, the diagrams on the right contribute to the discontinuity of the one on the left, namely $\Delta T_{12345} = \Delta T^{(2a)}_{12345} + \Delta T^{(2b)}_{12345} + \Delta T^{(3a)}_{12345} + \Delta T^{(3b)}_{12345}$.

4.4.1 Dispersion relation

The ideal of the dispersion relations is to transform a self-energy subloop into a one dimensional integral, based on the algorithm

$$B_0(p^2; m_1^2, m_2^2) = \frac{1}{2\pi} \int_{(m_1+m_2)^2}^{\infty} ds \frac{\Delta B_0(s; m_1^2, m_2^2)}{s - p^2 - i\epsilon}, \tag{4.10}$$

where $\Delta B_0(s; m_1^2, m_2^2)$ is the discontinuity of the function $B_0(p^2; m_1^2, m_2^2)$ along the branch cut from $s = (m_1 + m_2)^2$ to infinity in the s-complex plane. The discontinuity function can be given by the formula

$$\Delta B_0(s; m_1^2, m_2^2) = 2\pi i \left(\frac{s}{4\pi\mu}\right)^{-\varepsilon} \frac{\Gamma(1-\varepsilon)}{\Gamma(2-2\varepsilon)} \frac{\lambda^{\frac{1}{2}-\varepsilon}(s, m_1^2, m_2^2)}{s^{1-2\varepsilon}} \Theta\left(s - (m_1+m_2)^2\right),$$

where the Källén function $\lambda(x, y, z) = (x - y - z)^2 - 4yz$ and ε is from the dimension $d = 4 - 2\varepsilon$. A simple example is the sunset diagram in Figure 10

$$\begin{aligned} T_{234}(p^2; m_2^2, m_3^2, m_4^2) &= \left\langle\left\langle \frac{1}{(q_1+p)^2 - m_2^2} \frac{1}{q_2^2 - m_4^2} \frac{1}{(q_1+q_2)^2 - m_3^2} \right\rangle\right\rangle \\ &= \frac{1}{2\pi i} \int_{(m_2+m_3)^2}^{\infty} ds \left\langle \frac{1}{q_2^2 - m_4^2} \frac{\Delta B_0(s; m_2^2, m_3^2)}{s - (q_2+p)^2 - i\epsilon} \right\rangle \\ &= -\frac{1}{2\pi i} \int_{(m_2+m_3)^2}^{\infty} ds \Delta B_0(s; m_2^2, m_3^2) B_0(p^2; s, m_4^2), \end{aligned}$$

where the double bracket is defined in (5.15). It can be seen that the formula (4.10) transfers a self-energy sub-bubble into a one dimensional integration of a propagator with a momentum (q_2+p) and a mass s. That's the reason that it is advantageous for its high efficiency.

As an extension of the method of dispersion relation from the self-energy sub-loops, a master integral of two-loop self-energy Feynman amplitude of five propagators reads

$$\begin{aligned} T_{12345}(p^2; m_1^2, m_2^2, m_3^2, m_4^2, m_5^2) = \left\langle\left\langle \frac{1}{[q_1^2 - m_1^2][(q_1-p)^2 - m_2^2]} \right.\right. \\ \left.\left. \times \frac{1}{[(q_1+q_2)^2 - m_3^2][q_2^2 - m_4^2][(q_2+p)^2 - m_5^2]} \right\rangle\right\rangle. \end{aligned}$$

The integral T_{12345} can be obtained by integrating along the branch cuts

$$T_{12345}(p^2; m_1^2, ..., m_5^2) = \frac{1}{2\pi i}\int_{s_0}^{\infty} ds \frac{\Delta T_{12345}(s; m_1^2, ..., m_5^2)}{s - p^2 - i\epsilon},$$

where the discontinuity across the branch cuts is

$$\Delta T_{12345}(s; m_1^2, ..., m_5^2) = 2i\Im m \left[T_{12345}(p^2; m_1^2, ..., m_5^2)\right],$$

where $\Im m$ is the imaginary part of the argument. According to Cutkosky's rules [22], the discontinuity of the master integral is decomposed to four parts as depicted in Figure 11. The lines cut through by a dashed line indicate the corresponding propagators are replaced by delta functions in deriving its discontinuity function. The delta functions lead to a lower limit of the integration so that $s_0^{(2a)} = (m_1 + m_2)^2$, $s_0^{(2b)} = (m_4 + m_5)^2$, $s_0^{(3a)} = (m_2 + m_3 + m_4)^2$ and $s_0^{(3b)} = (m_1 + m_3 + m_5)^2$. Therefore, for instance, the contribution from the first diagram on the right hand side of Figure 11 to the master integral is

$$T_{12345}^{(2a)}(p^2; m_1^2, ..., m_5^2) = \frac{1}{2\pi i}\int_{s_0^{(2a)}}^{\infty} ds \frac{\Delta T_{12345}^{(2a)}(s; m_1^2, ..., m_5^2)}{s - p^2 - i\epsilon}.$$

The details will not be explored in this thesis, we refer to [21, 22, 5] for deeper discussions.

4.4.2 Integration by parts

The idea of the integration by parts (IBP) [25] is to obtain a series of equations of Feynman integrals by taking the derivative with respect to loop momenta, such that a class of the Feynman integrals can be expressed in terms of some master integrals. The equations of the integrals of derivatives originate from the boundary conditions

$$0 = \int d^d q \frac{\partial}{\partial q_\mu} f^\mu(q),$$

where $f^\mu(q)$ could be proportional to loop momentum q or some external momentum. By inserting different kernels $f^\mu(q)$, one can find as many equations from IBP as possible until a given integral can be reduced to irreducible integrals. We can take a simple case as an example. For a one-loop vacuum massive Feynman integrals, we denote

$$\Delta_n = \int \frac{d^d q}{(q^2 - m^2)^n}.$$

By exploring the IBP equations, we find

$$\int d^d q \frac{\partial}{\partial q^\mu} \frac{q^\mu}{(q^2 - m^2)^n} = 0.$$

It gives rise to

$$(d - 2n)\Delta_n - 2nm^2\Delta_{n+1} = 0,$$

so we have the recurrence relation

$$\Delta_n = \frac{d - 2n + 2}{2(n-1)m^2}\Delta_{n-1}.$$

Of course, the integrand may contain more than one propagator but, as long as we have sufficient IBP equations, a given Feynman integral can be further reduced to a minimal set of integrals. However, the difficulty of the method is that the master integrals may not be easily computed.

4.4.3 Sector decomposition

Another method which has been developed recently is called sector decomposition. We will concisely discuss the basic idea of the approach, for a broader content of the subject the readers are referred to [26]. Concerning collinear and soft divergences, we consider a d-dimensional scalar L-loop Feynman integral with N propagators. In general, after introducing Feynman parameters, the integral can be expressed in terms of a symmetric $L \times L$ matrix M_{jl}, a L-vector Q and a scalar J,

$$G = \Gamma(N) \int \prod_{i=1}^{N} dx_i \delta(1 - \sum_{i=1}^{N} x_i) \int \prod_{l=m}^{L} \frac{d^d k_m}{i\pi^{d/2}} \left[\sum_{j,l=1}^{L} k_j \cdot k_l M_{jl} - 2 \sum_{j=1}^{L} k \cdot Q_j + J \right]^{-N}.$$

Through integrating the loop momenta after shifting the the momenta to remove the linear term, the Feynman integral becomes

$$G = (-1)^N \Gamma(N - \frac{d}{2}L) \int_0^\infty \prod_{i=1}^{N} dx_i \delta(1 - \sum_{i=1}^{N} x_i) \frac{\mathcal{U}^{N-(L+1)\frac{d}{2}}}{\mathcal{F}^{N-L\frac{d}{2}}},$$

where

$$\begin{aligned} \mathcal{F}(x_1, ..., x_N) &= \det(M) \left[J - \sum_{j,l=1}^{L} Q_i \cdot Q_j M_{jl}^{-1} \right], \\ \mathcal{U}(x_1, ..., x_N) &= \det(M). \end{aligned}$$

For the first step of the sector decomposition, we divide the domain of the integration into N parts and integrate out the δ-function so that

$$\int_0^\infty \prod_{i=1}^{N} dx_i = \int_0^\infty \prod_{i=1}^{N} dx_i \prod_{j=1}^{N} \theta(x_j \geq 0) = \sum_{l=1}^{N} \int_0^\infty \prod_{i=1}^{N} dx_i \prod_{j=1, j\neq l}^{N} \theta(x_l \geq x_j \geq 0),$$

where the function $\theta(x \geq y) = 1$ if $x \geq y$ is true and zero otherwise. Then we do the substitution of the variables

$$x_j = \begin{cases} x_l t_j, & \text{if } j < l, \\ x_l, & \text{if } j = l, \\ x_l t_{j-1}, & \text{if } j > l. \end{cases}$$

Due to the homogeneity of the functions, $\mathcal{F}$ and $\mathcal{U}$, with variables x_j, x_j can factorize completely in the them. After integrating out the δ-function with respect to x_l, the Feynman integral G can be written as $G = (-1)^N \Gamma(N - \frac{d}{2}L) \sum_{l=1}^{N} G_l$, where

$$G_l = \int_0^1 \prod_{i=1}^{N-1} dt_i \frac{\mathcal{U}^{N-(L+1)\frac{d}{2}}}{\mathcal{F}_l^{N-\frac{d}{2}L}}.$$

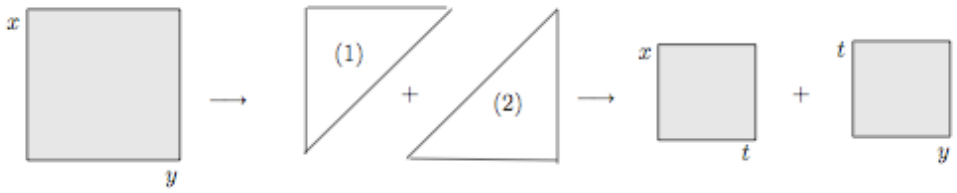

Figure 12: For a 2-dimension domain of (x, y), with the variable transform $y = xt$ for the region (1) and $x = yt$ for the region (2); the resulting domains of the respective variables are shown in the right.

The singularities are coming from the region of small t_i's, it will be obvious as we impose the next subdivision on them. Similarly, we decompose the domain of t_j into r divisions and apply the variable transform as below

$$\prod_{j=1}^{r}\theta(1\geq t_{\alpha_j}\geq 0)=\sum_{k=1}^{r}\prod_{j=1,j\neq k}^{r}\theta(t_{\alpha_k}\geq t_{\alpha_j}\geq 0),\;\; t_{\alpha_j}=\begin{cases}t_{\alpha_k}t_{\alpha}, & \text{if } j\neq k,\\ t_{\alpha_k}, & \text{if } j=k.\end{cases}$$

The determination of r will not be discussed here; the corresponding discussion is provided in [26]. A simple illustration of the decomposition of the domain of t_{α_j} is in Figure 12. Consequently, the integral in the sub-region which is labeled by (l, k) is in the form

$$G_{lk}=\int_0^1\prod_{i=1}^{N-1}dt_i\left(\prod_{j=1}^{N-1}t_j^{A_j-B_j\varepsilon}\right)\frac{\mathcal{U}_{lk}^{N-(L+1)\frac{d}{2}}}{\mathcal{F}_{lk}^{N-\frac{d}{2}L}},\qquad \begin{matrix}l=1,...,(N-1),\\ k=1,...,r,\end{matrix}\tag{4.11}$$

where A_j and B_j are integers and $G_l=\sum_{k=1}^{r}G_{lk}$. The reason that the factor $t_j^{A_j-B_j\varepsilon}$ can be factorized is also due to the homogeneity of the function $\mathcal{U}_{lk}$ and $\mathcal{F}_{lk}$. The integrand of the (4.11) can be characterized in the form

$$I_j=\int_0^1 dt_j t_j^{A_j-B_j\varepsilon}\mathcal{I}(t_j,\varepsilon).$$

It can be seen that for $A_j\geq 0$ the integral does not contain an ε-pole. For $A_j<0$, we then expand $\mathcal{I}(t_j,\varepsilon)$ into a Taylor series around $t_j=0$ up to the order $(|A_j|-1)$. In the end, we have

$$\mathcal{I}(t_j,\varepsilon)=\sum_{n=0}^{|A_j|-1}\mathcal{I}_j^{(n)}(0,\varepsilon)\frac{t_j^n}{n!}+R(t_j,\varepsilon),$$

where $R(t_j, \varepsilon)$ is the remainder term which does not have pole of ε. By integrating over t_j, we obtain

$$I_j = \sum_{n=0}^{|A_j|-1} \frac{1}{A_j + n + 1 - B_j\varepsilon} \frac{\mathcal{I}_j^{(n)}(0,\varepsilon)}{n!} + \int_0^\infty dt_j t_j^{A_j - B_j\varepsilon} R(t_j, \varepsilon).$$

Therefore, a logarithmic divergence produces a term proportional to $1/\varepsilon$ at $A_j = -1$ and $n = 0$. As the same procedure is applied on the rest of t_j until $j = N-1$, all the soft and collinear singularities can be isolated in the end.

5.0 DETAILS OF CALCULATIONS

5.1 FEYNARTS AND FEYNCALC

For the practical calculations of Feynman integrals, the use of the software routines are required due to the large number of the Feynman diagrams and the amount of algebraic work. To generate the Feynman diagrams of the process $Z \to b\bar{b}$, FeynArts is helpful. Some example diagrams generated by the FeynArts [30] are shown in Figure 13. Besides, FeynArts also helps to produce counterterms for multi-loop diagrams as well as their corresponding diagrams. After obtaining the amplitude from the FeynArts, the FeynCalc [31] provides functions for algebraic operations, like taking the trace of the Dirac matrices and contracting the space-time indices. Below, some useful commands are listed in the table.

5.2 CALCULATIONS OF WEAK MIXING ANGLE

5.2.1 Projection of vertex corrections

In the computations of the two-loop radiative corrections, all masses of the leptons and the quarks except the top quark are ignored, as well as the Yukawa couplings. Besides, the quark mixing matrix is taken as diagonal. The vector and axial-vector components, $\hat{v}_{\mathrm{f},\mu}$ and $\hat{a}_{\mathrm{f},\mu}$ of the vertex corrections, $\hat{z}_{\mathrm{f},\mu}$, are obtained by contracting with the projection operators

$$\hat{v}_{\mathrm{f},\mu}(k^2) = \frac{1}{2(2-d)k^2}\mathrm{Tr}[\gamma^\mu \not{p}_1 \hat{z}_{\mathrm{f},\mu}(k^2)\not{p}_2], \tag{5.1}$$

$$\hat{a}_{\mathrm{f},\mu(\mathrm{k}^2)} = \frac{1}{2(2-d)k^2}\mathrm{Tr}[\gamma^5\gamma^\mu \not{p}_1 \hat{z}_{\mathrm{f},\mu}(k^2)\not{p}_2], \tag{5.2}$$

where d is the dimension of the space-time, $p_i\,(i = 1, 2)$ are the outgoing momenta of the external fermions and k is the ingoing momentum of the Z boson. Thus $k^2 = M_Z^2$ and $p_i^2 = 0$ for b quarks. After the projections with the operators, there are integrals with tensor products in the numerators. These integrals have to be reduced to scalar integrals by different methods. In the fourth section, different approaches for the reduction of those tensor integrals are discussed.

5.2.2 Calculations with γ^5 matrix

In dimensional regularization, we have to do the tensor and $\gamma-$matrix calculations in the numerators for dimension d. Some of the relations can be derived from the algebras of γ matrices in d dimension, such as

$$\gamma^\mu\gamma_\mu = d,$$

which follows from $\{\gamma^\mu, \gamma^\nu\} = 2g^{\mu\nu}$. Similarly,

$$\gamma_\mu \not{a}\not{b}\gamma^\mu = 4a\cdot b + (d-4)\not{a}\not{b}, \tag{5.3}$$
$$\gamma_\mu \not{a}\not{b}\not{c}\gamma^\mu = -2\not{c}\not{b}\not{a} + (d-4)\not{a}\not{b}\not{c}. \tag{5.4}$$

However, the relation of the matrix γ^5 satisfying $\{\gamma^\mu, \gamma^5\} = 0$ in 4 dimensions can not be extended to d-dimensions. Let's consider the equalities literally,

$$\mathrm{Tr}[\gamma_5\gamma_\mu\gamma^\mu] = d\mathrm{Tr}[\gamma_5] = -\mathrm{Tr}[\gamma_\mu\gamma_5\gamma^\mu] = -\mathrm{Tr}[\gamma_5\gamma^\mu\gamma_\mu] = -d\mathrm{Tr}[\gamma_5],$$

where the anti-commutativity of γ_5 and the trace cyclicity have been used. So that it shows $\mathrm{Tr}[\gamma_5] = 0$ for $d \neq 0$. Besides, with the help of (5.3),

$$\mathrm{Tr}[\gamma_5\gamma_\mu\gamma^\mu\gamma^\alpha\gamma^\beta] = d\mathrm{Tr}[\gamma_5\gamma^\alpha\gamma^\beta] = -\mathrm{Tr}[\gamma_5\gamma^\mu\gamma^\alpha\gamma^\beta\gamma_\mu] = -(d-4)\mathrm{Tr}[\gamma_5\gamma^\alpha\gamma^\beta],$$

leading to $(d-2)\mathrm{Tr}[\gamma_5\gamma^\alpha\gamma^\beta] = 0$. Hence $\mathrm{Tr}[\gamma_5\gamma^\alpha\gamma^\beta] = 0$ for $d \neq 2$. In the similar way, from (5.4)

$$\begin{aligned}&\mathrm{Tr}[\gamma_5\gamma_\mu\gamma^\mu\gamma^\alpha\gamma^\beta\gamma^\gamma\gamma^\delta] = d\mathrm{Tr}[\gamma_5\gamma^\alpha\gamma^\beta\gamma^\gamma\gamma^\delta] = -\mathrm{Tr}[\gamma_5\gamma^\mu\gamma^\alpha\gamma^\beta\gamma^\gamma\gamma^\delta\gamma_\mu]\\ &= -(d-8)\mathrm{Tr}[\gamma_5\gamma^\alpha\gamma^\beta\gamma^\gamma\gamma^\delta],\end{aligned}$$

which states that $\mathrm{Tr}[\gamma_5\gamma^\alpha\gamma^\beta\gamma^\gamma\gamma^\delta] = 0$ for $d \neq 4$. The procedures can go on, and the conclusion is that all the traces with γ_5 vanish if d is not an even integer. However, it contradicts the requirement that γ_5 satisfies in 4-dimension, namely

$$\mathrm{Tr}[\gamma_5\gamma^\alpha\gamma^\beta\gamma^\gamma\gamma^\delta] = 4i\epsilon^{\alpha\beta\gamma\delta}. \tag{5.5}$$

In QED and QCD, there is no γ_5 in the Lagrangian, so no problem arises. However, one encounters difficulties when considering the electroweak theory. Fortunately, the renormalizability of the Standard Model requires that the parts involving (5.5) have to be UV finite in two-loop diagrams. Therefore, the computation is separated into two parts: the one without the contributions from γ_5 is dealt with by the dimensional regularization, the other is computed independently in 4-dimension [21].

5.2.3 Pole Scheme for Z resonance

As to the calculations of the radiative corrections for the mixing angle of $Z \to b\bar{b}$, a method proven to be gauge invariant and unitary is the pole-scheme [32, 33, 34]. In the process $e^+e^- \to f\bar{f}$, near the Z-pole, the amplitude can be written as

$$\mathcal{A}[e^+e^- \to f\bar{f}] = \frac{R}{s - \mathcal{M}_Z^2} + S + (s - \mathcal{M}_Z^2)S' + ..., \tag{5.6}$$

where $\mathcal{M}_Z^2 = \overline{M}_Z^2 - i\overline{M}_Z\overline{\Gamma}_Z$. All coefficients of Laurent expansion, $R, S, S', ...$ and the pole location $\mathcal{M}_Z^2$ are individually gauge invariant. The first term in (5.6) corresponds to the Breit-Wigner formula of the Z resonance line shape, as discussed in Chapter 2. Experimentally, the Z boson mass [35] is determined by the mass parameter of the Breit-Wigner function with an energy-dependent width

$$\mathcal{A} \propto \frac{1}{s - M_Z^2 + is\Gamma_Z/M_Z}. \tag{5.7}$$

After comparing the mass parameters in (5.6) and (5.7), we can obtain $\mathcal{M}_Z^2 = \frac{M_Z^2}{1 - i\Gamma_Z/M_Z}$, so that the theoretical $\overline{M}_Z^2$ and the experimental M_Z^2 are related to each other by

$$\overline{M}_Z^2 = M_Z^2/(1 + \Gamma_Z^2/M_Z^2). \tag{5.8}$$

The relation between these two values is

$$\overline{M}_Z = M_Z - 34.1\,\text{MeV}.$$

The information for the effective mixing angle is included in the pole residue R in (5.6). In our calculations, the masses of the quarks are assumed to be zero except the top quark, so that some of the Lorentz structures diminish, such as the electro-magnetic moment. Introduce the following notation for vertex and self-energy form factors for nonzero Lorentz structures:

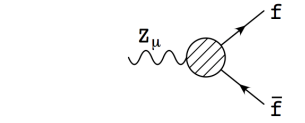

$$\equiv \quad \Gamma[Z_\mu f\bar{f}] \equiv z_{\mathrm{f},\mu} \equiv i\gamma^\mu(v_\mathrm{f} + a_\mathrm{f}\gamma_5),$$

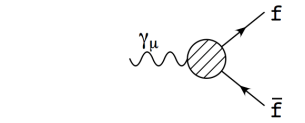

$$\equiv \quad \Gamma[A_\mu f\bar{f}] \equiv g_{\mathrm{f},\mu} \equiv i\gamma^\mu(q_\mathrm{f} + p_\mathrm{f}\gamma_5),$$

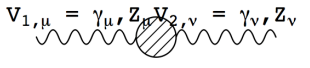

$$\equiv \quad \Sigma^{\mu\nu}_{V_1V_2}, \tag{5.9}$$

where the blobs stands for one-particle irreducible n-point functions. Some examples for the two-loop diagrams that will be computed are shown in the following.

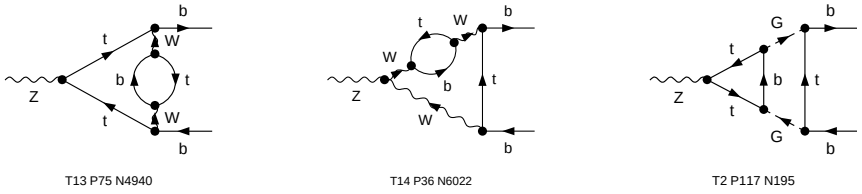

(a) (b) (c)

Figure 13: Some examples in the calculations of two-loop rediative corrections for $Z \to b\bar{b}$, where G stands for the Goldstone boson in (c).

With above definitions, up to next-to-next-to-leading order, the residue R is expressed in the form

$$\begin{aligned}
R &= z_{\rm e}^{(0)} R_{ZZ} z_{\rm f}^{(0)} + \left[\hat{z}_{\rm e}^{(1)}(M_Z^2) z_{\rm f}^{(0)} + z_{\rm e}^{(0)} \hat{z}_{\rm f}^{(1)}(M_Z^2)\right] \left[1 + \Sigma_{\gamma Z}^{(1)\prime}(M_Z^2)\right] \\
&\quad + \hat{z}_{\rm e}^{(2)}(M_Z^2) z_{\rm f}^{(0)} + z_{\rm e}^{(0)} \hat{z}_{\rm f}^{(2)}(M_Z^2) + \hat{z}_{\rm e}^{(1)}(M_Z^2) \hat{z}_{\rm f}^{(1)}(M_Z^2) \\
&\quad - i M_Z \Gamma_Z \left[\hat{z}_{\rm e}^{(1)\prime}(M_Z^2) z_{\rm f}^{(0)} + z_{\rm e}^{(0)} \hat{z}_{\rm f}^{(1)\prime}(M_Z^2)\right], \\
R_{ZZ} &= 1 - \Sigma_{ZZ}^{(1)\prime}(M_Z^2) \\
&\quad - \Sigma_{ZZ}^{(2)\prime}(M_Z^2) + \left(\Sigma_{ZZ}^{(1)\prime}(M_Z^2)\right)^2 + i M_Z \Gamma_Z \Sigma_{ZZ}^{(1)\prime\prime}(M_Z^2) \\
&\quad - \frac{1}{M_Z^4} \left(\Sigma_{\gamma Z}^{(1)\prime}(M_Z^2)\right)^2 + \frac{2}{M_Z^2} \Sigma_{\gamma Z}^{(1)}(M_Z^2) \Sigma_{\gamma Z}^{(1)\prime}(M_Z^2).
\end{aligned}$$

According to the definition of $\sin\theta_{\rm eff}^{\rm f}$ in (2.21), the effective weak mixing angle can be derived from the residue R as

$$\begin{aligned}
\sin\theta_{\rm eff}^{\rm f} &\equiv \left(1 - \frac{\overline{M}_{\rm W}^2}{\overline{M}_{\rm Z}^2}\right) {\rm Re}\{1 + \Delta\overline{\kappa}_{\rm Z}^{\rm f}(M_Z^2)\} \\
&= \left(1 - \frac{\overline{M}_{\rm W}^2}{\overline{M}_{\rm Z}^2}\right) {\rm Re} \left\{ 1 + \left. \frac{\hat{a}_{\rm f}^{(1)} v_{\rm f}^{(0)} - \hat{v}_{\rm f}^{(1)} a_{\rm f}^{(0)}}{a_{\rm f}^{(0)}(a_{\rm f}^{(0)} - v_{\rm f}^{(0)})} \right|_{k^2 = M_Z^2} \right. \\
&\quad \left. + \left. \frac{\hat{a}_{\rm f}^{(2)} v_{\rm f}^{(0)} a_{\rm f}^{(0)} - \hat{v}_{\rm f}^{(2)} (a_{\rm f}^{(0)})^2 - (\hat{a}_{\rm f}^{(1)})^2 v_{\rm f}^{(0)} + \hat{a}_{\rm f}^{(1)} \hat{v}_{\rm f}^{(1)} a_{\rm f}^{(0)}}{(a_{\rm f}^{(0)})^2 (a_{\rm f}^{(0)} - v_{\rm f}^{(0)})} \right|_{k^2 = M_Z^2} \right\}.
\end{aligned} \tag{5.10}$$

5.2.4 Corrections of Partial Width

In theory, the Z decay widths, which contain various contributions from the radiative corrections, are described for the processes of $Z \to f\bar{f}$ as

$$\Gamma_{f\bar{f}} \;=\; N_c^f \frac{G_F M_Z^3}{6\sqrt{2}\pi} \left(|a_f|^2 \mathcal{R}_{\mathrm{A}f} + |v_f|^2 \mathcal{R}_{\mathrm{V}f} \right),$$

where $\mathcal{R}_{Af}$ and $\mathcal{R}_{Vf}$ are the radiator factors including the final state corrections of QED and QCD [36, 37]. They can be denoted in terms of N-loop corrections, like in (2.15) and (2.16), as follows

$$\mathcal{R}_{\mathrm{A}f} = 1 + \mathcal{R}_{\mathrm{A}f}^{(1)} + \mathcal{R}_{\mathrm{A}f}^{(2)} + \cdots, \qquad \mathcal{R}_{\mathrm{V}f} = 1 + \mathcal{R}_{\mathrm{V}f}^{(1)} + \mathcal{R}_{\mathrm{V}f}^{(2)} + \cdots.$$

The values of the above up to the next-to-next leading order can be found in [36, 37]. The branching ratios for those primary quarks which can be identified in final states are defined as

$$R_q \equiv \frac{\Gamma_{q\bar{q}}}{\Gamma_{\mathrm{had}}}, \text{ where } \Gamma_{\mathrm{had}} = \Gamma_{u\bar{u}} + \Gamma_{d\bar{d}} + \Gamma_{s\bar{s}} + \Gamma_{c\bar{c}} + \Gamma_{b\bar{b}}. \tag{5.11}$$

As the approximations, $\Gamma_{u\bar{u}} \sim \Gamma_{c\bar{c}}$ and $\Gamma_{d\bar{d}} \sim \Gamma_{s\bar{s}}$, are used, the branching ratio becomes $R_b = 1/(1 + \frac{2(\Gamma_{d\bar{d}}+\Gamma_{u\bar{u}})}{\Gamma_{b\bar{b}}})$. Its corrections up to the next-to-next-leading order can be obtained through

$$\begin{aligned}
\frac{\Gamma_q}{\Gamma_b} \;=\; & \frac{G_q^{(0)}}{G_b^{(0)}} + \frac{2}{(G_b^{(0)})^2} \Re e \left\{ G_b^{(0)} G_q^{(1)} - G_q^{(0)} G_b^{(1)} \right\} + \frac{1}{(G_b^{(0)})^2} \left(G_b^{(0)} \mathcal{R}_b^{(0)} - G_b^{(0)} \mathcal{R}_b^{(0)} \right) \\
& + \frac{1}{(G_b^{(0)}))^3} \Re e \Big\{ (G_b^{(0)})^2 [2G_q^{(2)} + (a_q^{(1)})^2 + (v_q^{(1)})^2] \\
& - G_b^{(0)} G_q^{(0)} [2G_b^{(2)} + (a_b^{(1)})^2 + (v_b^{(1)})^2] - 4G_q^{(0)} G_q^{(0)} G_q^{(0)} + 4G_q^{(0)} (G_q^{(0)})^2 \Big\} \\
& + \frac{1}{(G_b^{(0)})^2} [G_b^{(0)} \mathcal{R}_q^{(2)} - G_q^{(0)} \mathcal{R}_b^{(2)} - G_b^{(0)} \mathcal{R}_q^{(1)} \mathcal{R}_b^{(1)} + G_q^{(0)} (\mathcal{R}_b^{(1)})^2] \\
& + \frac{2}{(G_b^{(0)})^3} \Big[(G_b^{(0)})^2 (a_q^{(0)} a_q^{(1)} \mathcal{R}_{A,q}^{(1)} + v_q^{(0)} v_q^{(1)} \mathcal{R}_{V,q}^{(1)}) - G_b^{(0)} G_b^{(1)} \mathcal{R}_q^{(1)} \\
& + G_q^{(0)} G_b^{(1)} \mathcal{R}_b^{(1)} + G_q^{(0)} a_b^{(0)} v_b^{(0)} (a_b^{(0)} v_b^{(1)} + v_b^{(0)} a_b^{(1)}) (\mathcal{R}_{A,b}^{(1)} - \mathcal{R}_{V,b}^{(1)}) \\
& - G_b^{(0)} G_q^{(1)} \mathcal{R}_b^{(1)} \Big],
\end{aligned} \tag{5.12}$$

where $G_f^{(n)} = a_f^{(0)} a_f^{(n)} + v_f^{(0)} v_f^{(n)}$ and $\mathcal{R}_f^{(n)} = (a_f^{(0)})^2 \mathcal{R}_{A,f}^{(n)} + (v_f^{(0)})^2 \mathcal{R}_{V,f}^{(n)}$.

5.3 REDUCTION OF TENSOR INTEGRALS

With the help of the routines mentioned in the previous section, what are left are various tensor integrals which take extra work to reduce to scalar integrals, if possible. There are several methods for the tensor reduction; one of the approaches is Passarino and Veltman's (PV) [19], which exploits Lorentz covariance of the integrals for tensor decomposition; another method is the integration by parts (IBP). In fact, those methods mentioned above might not be useful for some of the tensor integrals. For instance, as will be shown in the following section, the PV method can always decompose the tensor integrals of the self-energy diagrams, but might not work out for other types of diagrams. Therefore, for those problematic integrals, which can not be transformed into scalar integrals by either the PV or the IBP method, the Mellin-Barnes representations are helpful dealing with the numerical calculations. In the following, some of those approaches are discussed briefly.

5.3.1 Reduction of two-loop self-energies tensor integrals

As depicted in Chapter 3, the self-energies of the gauge bosons are needed to cancel the UV divergences through the renormalization conditions. In order to decompose the tensor integrals into scalar ones, we define the unrenormalized self-energy of the gauge bosons

$$\Sigma^{\alpha\beta}_{\mu\nu}(k) = \left(-g_{\mu\nu} + \frac{k_\mu k_\nu}{k^2}\right)\Sigma^{\alpha\beta}_T(k^2) - \frac{k^\mu k^\nu}{k^2}\Sigma^{\alpha\beta}_L(k^2), \tag{5.13}$$

where α, β could be γ, Z or $W^\pm$ bosons. The transverse part $\Sigma^{\alpha\beta}_T(k^2)$ and the longitudinal part $\Sigma^{\alpha\beta}_L(k^2)$ can be extracted as

$$\begin{aligned}
\Sigma^{\alpha\beta}_T(k^2) &= \frac{1}{d-1}\left(-g_{\mu\nu} + \frac{k_\mu k_\nu}{k^2}\right)\Sigma^{\alpha\beta}_{\mu\nu}(k), \\
\Sigma^{\alpha\beta}_L(k^2) &= -\frac{k_\mu k_\nu}{k^2}\Sigma^{\alpha\beta}_{\mu\nu}(k).
\end{aligned}$$

The unrenormalized self-energies of fermions are decomposed into a vector, an axial vector, a scalar and a pseudo-scalar part similar to (3.4) as below,

$$\Sigma^f(p) = \not{p}\Sigma^f_V(p^2) + \not{p}\gamma_5\Sigma^f_A(p^2) + m_f\Sigma^f_S(p^2) + m_f\gamma_5\Sigma^f_P(p^2). \tag{5.14}$$

Each of the components can be obtained via

$$\Sigma^f_V(p^2) = \frac{1}{4p^2}\mathrm{Tr}\left[\not{p}\Sigma(p)\right],\ \Sigma^f_A(p^2) = \frac{1}{4p^2}\mathrm{Tr}\left[\gamma_5\not{p}\Sigma(p)\right],$$

and

$$\Sigma^f_S(p^2) = \frac{1}{4m}\mathrm{Tr}\left[\Sigma(p)\right],\ \Sigma^f_P(p^2) = \frac{1}{4m}\mathrm{Tr}\left[\gamma_5\Sigma(p)\right].$$

With the tensor decomposition stated as above the computation work is left to the scalar Feynman integrals which have scalar product of momenta, like $(q_1 \cdot q_2)$, $(p_1 \cdot q_1)$, etc., in the numerators. For doing those integrals, let us define some shorthand notations

$$\langle\langle ... \rangle\rangle = \int \frac{d^d q_1}{i\pi^2 (2\pi)^{d-4}} \int \frac{d^d q_2}{i\pi^2 (2\pi)^{d-4}} (...), \tag{5.15}$$

where q_1 and q_2 are the loop momenta of the integrals. Hence, a Feynman integral can be expressed as

$$T_{i_1 i_2 ... i_l}(p^2; m_1^2, m_2^2, ..., m_l^2) = \langle\langle \frac{1}{[k_{i_1}^2 - m_1^2][k_{i_2}^2 - m_2^2]...[k_{i_l}^2 - m_l^2]} \rangle\rangle,$$

where k_i is the momentum of the corresponding propagator, and will be related to q_1 and q_2. Let us denote this type of integral as T-integral. Some of the possible topologies of two-loop self-energy diagrams are presented in Figure 15. If there is a massless propagator, a prime is added to the corresponding subindex, e.g.

$$T_{1'23}(p^2; 0, m_2^2, m_3^2) = \langle\langle \frac{1}{k_1^2 [k_2^2 - m_2^2][k_3^2 - m_3^2]} \rangle\rangle.$$

For a convenient reason of the later use, the above integrand can be denoted as

$$\Delta_{1'23} \equiv \frac{1}{k_1^2 [k_2^2 - m_2^2][k_3^2 - m_3^2]}.$$

The master integral which has five propagators with different momenta and masses in Figure 14 can be denoted as

$$T_{12345}(p^2; m_1^2, m_2^2, ..., m_5^2) = \langle\langle \frac{1}{[k_1^2 - m_1^2][k_2^2 - m_2^2][k_3^2 - m_3^2][k_4^2 - m_4^2][k_5^2 - m_5^2]} \rangle\rangle,$$

Based on the momentum conservation, those momenta can be expressed as followsz

$$k_1 = q_1,\ k_2 = q_1 + p,\ k_3 = q_2 - q_1,\ k_4 = q_2,\ k_5 = q_2 + p.$$

In addition, T-Integrals possess symmetries, like they are invariant under the permutations (12)(45), (14)(25) and (15)(24). From the relations presented above, the scalar products can be expressed as sum of momentum squares, e.g.

$$(k_1 \cdot p) = \frac{1}{2}(k_2^2 - k_1^2 - p^2).$$

All of the k_i^2 can be canceled against the corresponding propagator through

$$k_i^2 = (k_i^2 - m_i^2) + m_i^2.$$

By the above formulas, integrals with scalar products in the numerator may be expressed by other T-integrals. However, some integrals can not be reduced further by the above treatment, they are called Y-Integrals. We present an example to show how these can be reduced; consider the integral

$$\langle\langle (p \cdot k_2) \Delta_{2345} \rangle\rangle \tag{5.16}$$

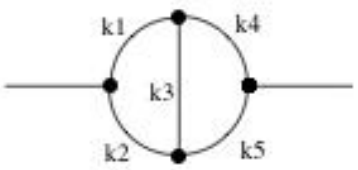

Figure 14: The topology of the master integral.

According to the Passarino-Veltman procedure for one-loop integrals, consider the sub-loop integral $\langle \Delta_{23} \rangle$ in the topologies of T_{2345}. So we may assume

$$\langle k_2^\mu \Delta_{23} \rangle = k_5^\mu s(k_5^2),$$

with the notation,

$$\langle ... \rangle = \int \frac{d^d q_1}{i\pi^2 (2\pi)^{d-4}} (...).$$

k_5^2 is the external momentum of the sub-loop bubble Δ_{23} and $s(k_5^2)$ is a Lorentz scalar. Solving for the Lorentz scalar, we obtain

$$s(k_5^2) = \frac{1}{k_5^2} \langle (k_5 \cdot k_2) \Delta_{23} \rangle = \langle (k_5 \cdot k_2) \Delta_{235'} \rangle.$$

Since the scalar product can be expressed as a sum of squared momenta

$$(k_5 \cdot k_2) = \frac{1}{2}(k_2^2 - k_3^2 + k_5^2), \tag{5.17}$$

$s(k_5^2)$ can be explicitly solved as

$$s(k_5^2) = \frac{1}{2} \left(\langle \Delta_{35'} \rangle - \langle \Delta_{25'} \rangle + \langle \Delta_{23} \rangle \right) + \frac{1}{2}(m_2^2 - m_3^2).$$

We may insert the above results back into the integral that we consider in the first place with the formula

$$(p \cdot k_5) = \frac{1}{2}(k_5^2 - k_4^2 + p^2),$$

and reach an expression in terms of T-integrals. As for the Y-integrals of higher rank, we may consider the case

$$\langle\langle (p\cdot k_2)(p\cdot k_2)\Delta_{2345}\rangle\rangle = p_\mu p_\nu \langle\Delta_{45}\langle k_5^\mu k_5^\nu \Delta_{23}\rangle\rangle, \tag{5.18}$$

so that with the same assumption as that of the first rank it can be written, for the sub-loop bubble,

$$\langle k_5^\mu k_5^\nu \Delta_{23}\rangle = A(k_5^2) g^{\mu\nu} + B(k_5^2) k_5^\mu k_5^\nu, \tag{5.19}$$

where $A(k_5^2)$ and $B(k_5^2)$ are Lorentz scalars. Eq. (5.19) can be contracted with $g_{\mu\nu}$ and $k_{5\mu}k_{5\nu}$ and give two equations for the scalar functions A and B,

$$\begin{aligned} A(k_5^2)d + B(k_5^2)k_5^2 &= \langle k_5^2 \Delta_{23}\rangle \\ A(k_5^2)k_5^2 + B(k_5^2)k_5^4 &= \langle (k_2\cdot k_5)^2 \Delta_{23}\rangle. \end{aligned}$$

For solving for the unknowns, $A(k_5^2)$ and $B(k_5^2)$, the factor $1/k_5^2$ can be regarded as a massless propagator. After inserting the above solutions back into Eq. (5.18) with the formula (5.17), we will obtain the tensor reduction integrals for the second rank.

5.3.2 Mellin-Barnes representation for tensor integrals

In the last section, the decomposition of the tensor integrals was discussed; however, in some occasions, the method does not apply. For example, consider the two-loop Feynman integral in Figure 16 with a scalar product $(q_2\cdot p_1)$ in the numerator

$$\begin{aligned} \langle\langle (q_2\cdot p_1)\Delta_{23456}\rangle\rangle &= \langle\langle \frac{(q_2\cdot p_1)}{[(q_1-p_2)^2-m_2^2][(q_1-p_1-p_2)^2-m_3^2]} \\ &\quad \times \frac{1}{[q_2^2-m_4^2][(q_1+q_2)^2-m_5^2][(q_1-p_1-p_2)^2-m_6^2]}\rangle\rangle, \end{aligned}$$

where p_1 and p_2 are the outgoing momenta on the right side of Figure 16. The integral can not be reduced to master integrals from the methods stated above. for those integrals, the Mellin-Barnes representation for the integrals with tensor products in the numerator are introduced in the section 4.1. In principle, the scalar integrals reduced by the PV method are simpler and could be computed more easily than those by the MB, which is advantageous in its generality but is slow in numerical calculations. Simple scalar integrals could be evaluated analytically or by the numerical methods discussed in section 4.4, such as the dispersion relation, etc. with great precision and efficiency. Therefore, our strategy of numerical calculations that we adopt is to use Passarino and Veltman's with priority; the MB is our second option. We consider a simple case as an example. For a one-loop tensor integral of rank 2 with 3 external legs,

$$I_{3,2} = \int \frac{d^dk}{i\pi^{\frac{d}{2}}} \frac{k^\mu k^\nu}{\left[(k+q_1)^2-m_1^2\right]\left[(k+q_2)^2-m_2^2\right]\left[(k+q_3)^2-m_3^2\right]},$$

where $q_1=0$, $q_2=p_1$ and $q_3=p_1+p_2$. Then introduce Feynman parameters for the denominator. We have

$$I_{3,2} = \Gamma(3)\int \frac{d^dk}{i\pi^{\frac{d}{2}}} \int \left(\prod_{i=1}^3 dx_i\right)\delta\left(1-\sum_{i=1}^3 x_i\right)\frac{k^\mu k^\nu}{\left[(k+P)^2-\Delta\right]^3}, \tag{5.20}$$

where

$$P = \sum_{i=1}^{3} x_i q_i, \text{ and } \Delta = \sum_{i=1}^{3} x_i m_i^2 + \sum_{j=2}^{3} \sum_{i<j} x_i x_j \left[-(q_i - q_j)^2 \right].$$

Shift the loop momentum, $k = K - P$, Eq. (5.20) becomes

$$I_{3,2} = \Gamma(3) \int \frac{d^d K}{i\pi^{\frac{d}{2}}} \int \left(\prod_{i=1}^{3} dx_i \right) \delta \left(1 - \sum_{i=1}^{3} x_i \right) \frac{K^\mu K^\nu - P^\mu K^\nu - K^\mu P^\nu + P^\mu P^\nu}{\left[K^2 - \Delta \right]^3}.$$

From the above, it is obvious that now the problem is to integrate the tensor integral, such as,

$$\int \frac{d^d K}{i\pi^{\frac{d}{2}}} \frac{K^\mu K^\nu}{\left[K^2 - \Delta \right]^3}, \quad \int \frac{d^d K}{i\pi^{\frac{d}{2}}} \frac{K^\mu}{\left[K^2 - \Delta \right]^3}, \cdots.$$

The integrals with tensor products in the numerator with an odd number of the new loop momentum K^μ are zero apparently; those integrals with even numbers of K^μ are proportional to the products of the metric tensor $g_{\mu\nu}$ due to the Lorentz Invariance. For instance, for an arbitrary power of the denominator, n,

$$\int \frac{d^d K}{i\pi^{\frac{d}{2}}} \frac{K^\mu K^\nu}{\left[K^2 - \Delta \right]^n} = C_{K^\mu K^\nu} g^{\mu\nu},$$

where $C_{K_\mu K\nu}$ is a constant. Contracting with $g_{\mu\nu}$, we can obtain

$$C_{K^\mu K^\nu} = \int \frac{d^d K}{i\pi^{\frac{d}{2}}} \frac{1}{\left[K^2 - \Delta \right]^{n-1}} + \Delta \int \frac{d^d K}{i\pi^{\frac{d}{2}}} \frac{1}{\left[K^2 - \Delta \right]^n}.$$

Both of the integrals can be calculated by Wick rotation [40]; the formula can be easily found in the textbooks of field theory, namely

$$\int \frac{d^d K}{i(2\pi)^d} \frac{1}{\left[K^2 - \Delta \right]^n} = \frac{(-1)^n}{(4\pi)^{d/2}} \frac{\Gamma(n - \frac{1}{2})}{\Gamma(n)} \left(\frac{1}{\Delta} \right)^{n - \frac{d}{2}}. \tag{5.21}$$

For the other tensor integral,

$$\int \frac{d^d K}{i\pi^{\frac{d}{2}}} \frac{K^\mu K^\nu K^\gamma K^\sigma}{\left[K^2 - \Delta \right]^n} = C_{K^\mu K^\nu K^\gamma K^\sigma} (g^{\mu\nu} g^{\gamma\sigma} + g^{\mu\gamma} g^{\nu\sigma} + g^{\mu\sigma} g^{\nu\gamma}).$$

After contracting with two metric tensors,

$$\begin{aligned} C_{K^\mu K^\nu K^\gamma K^\sigma} &= \frac{1}{d(d+2)} \int \frac{d^d K}{i\pi^{\frac{d}{2}}} \frac{K^4}{\left[K^2 - \Delta \right]^n} \\ &= \frac{1}{d(d+2)} \int \frac{d^d K}{i\pi^{\frac{d}{2}}} \frac{1}{\left[K^2 - \Delta \right]^{n-2}} + \frac{2\Delta}{d(d+2)} \int \frac{d^d K}{i\pi^{\frac{d}{2}}} \frac{1}{\left[K^2 - \Delta \right]^{n-1}} \\ &\quad + \frac{\Delta^2}{d(d+2)} \int \frac{d^d K}{i\pi^{\frac{d}{2}}} \frac{1}{\left[K^2 - \Delta \right]^n}. \end{aligned}$$

The integrals in the right hand side can be also computed with (5.21). Then those scalar integral are transformed into the Mellin-Barnes representations, as discussed in Chapter 4, and the numerical integration works can be finished by the MC numerical techniques in a similar way as discussed in Chapter Four.

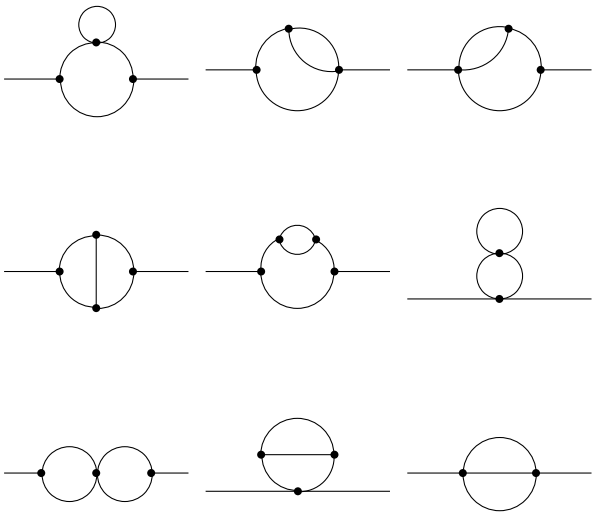

Figure 15: The possible topologies of the two-loop self-energies.

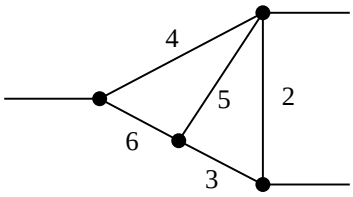

Figure 16: An example of a Feynman diagram with scalar products that need the Mellin-Barnes method.

6.0 RESULTS

In the previous chapters, we have discussed the renormalization theory in the SM and various numerical methods of calculating the Feynman integrals. Before going into the numerical calculations, there are several steps which have to be taken. The first is to generate fermionic Feynman diagrams for the process $Z \to b\bar{b}$ with FeynArts, and perform the Dirac algebra with FeynCalc in order to obtain the form factors. Secondly, two tensor reduction methods are processed to acquire scalar integrals. Then the numerical computations can be executed. As a main tool in this project, the Mellin-Barnes representation is introduced, and distinctive approaches of making the complex integration converge with a better efficiency are developed. In the first section of this chapter, we present the numerical results of the MB with examples. They will show that the developed routines for the MB are efficient for the two-loop Feynman diagrams. In the second section, the calculations of the weak mixing angle and the branching ratio for the process $Z \to b\bar{b}$ are applied with different routines. In general, the PV method is very efficient, but only works for relatively simple integrals. The MB method is not limited to certain types of diagrams; however, the integrations of high dimension are slow in convergence. Therefore, we have to apply both routines in order to aquire an efficient computation. For the two physical quantities shown in our results, $\sin\theta^{b\bar{b}}_{\text{eff}}$ and R_b, the weak mixing angle with a fermionic loop has been computed [6], and R_b has not yet. Therefore, our numerical outcomes have to show the agreement with the numbers that have been published for $\sin\theta^{b\bar{b}}_{\text{eff}}$, so that it could corroborate the validity of our calculations of R_b.

6.1 RESULTS AND COMPARISON

In this section, the results of two diagrams, as shown in Fig 17, are presented, different numerical methods are used to compute the complex integrals derived from the Cauchy theorem in the MB representations. For integrations with fewer variables, like not greater than three, the method of Gaussian Quadrature is applied. As in the case of the sunset diagram, Fig 17 (a), the integrals has three, two and one dimensional complex integrals. In each dimension, it is divided into cells of two unit length, and $30 \sim 40$ gaussian points are adopted in each cell. The most time-consuming integral, of course, the three dimensional one, takes less than 20 minutes to reach an acceptable accuracy. The comparison with the other method and the results are shown in Table 6.1. In principle, for the high dimensional integrations, they are difficult to converge without any additional treatment, especially when there is a exponential factor $(-1)^z$ in the integrand when $Q^2 < 0$, as in Eq. (4.4). The problem stays even with variable changes and the contour deformation as discussed in Section 4.2, since the factor makes the function oscillate and decrease at a slow rate and too many integration variables take more sample points in the integration. The way to solve it is to

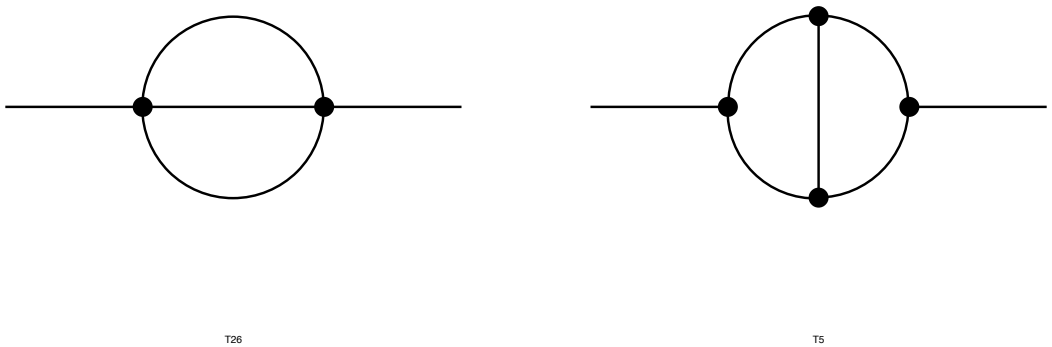

(a) (b)

Figure 17: Fig (a): Sunset diagram; Fig (b): Five propagator self-energy diagram.

reduce the dimensions with the formulae as proposed in Section 4.2.2. For example, in the case of the Fig. 17 (b), the 10 dimensional complex integral is applied with Eq. (4.7) three times and Eq. (4.8) once. Another complex integral of nine variables due to a pole which crosses the chosen contours could also be applied by the same reduction formulas. Therefore in the actual numerical computation we just need to deal with a 6 and a 5 dimensional integral, as shown in Table 2, instead of those of higher than 9 dimensions as long as the reduction processes are satisfied with all the requirements on their contours. Normally, with one variable less, the integral could converge ten times faster for the same targeted precision, so the reduction method is an essential step in the whole procedure. Based on the above method with the contour deformation, even with the integral with the exponential factor it takes about 60 minutes to reach an error smaller than 1% with a 2.4 GHz CPU. As for the integrals without the exponential growth factor, their errors can improve one more digit in about the same amount of time. When compared with the results from the method of dispersion relation, they are consistent within Monte Carlo errors to relatively smaller differences.

	$(m_1^2, m_2^2, m_3^2, q^2)$	MB Result	D.R. Result	precision
1	(2, 5, 3, 14)	30.14577811533	30.1458206548267	1.41×10^{-6}
2	(1, 1.5, 1.2, 20)	13.30962019836	13.3096129704	5.43×10^{-7}
		$-4.356016497i$	$-4.35599326485i$	53.3×10^{-7}

Table 1: The finite parts of sunset integrals of three dimensional, two dimensional and one dimensional integrals are computed with Gaussian Quadrature as a low dimensional example. D.R. result, which is from the method of dispersion relation, is presented for comparison.

	$(m_1^2, ..., m_5^2, q^2)$	MB Result	D.R. Result	error %	Vegas errors
1	(1, 1, 1, 1, 1,20)	0.440305	0.43951728	0.179%	0.21%, 0.42%
		$-0.255021i$	$-0.25364547i$	0.542%	0.37%, 0.73%
2	(1, 1, 1, 2, 2,20)	0.442884	0.44073958	0.487%	0.36%, 0.77%
		$-0.347932i$	$-0.34899118i$	-0.303%	0.29%, 0.60%
3	(1, 1, 1, 1, 1,20)	0.0	0.43951728	100%	0.0%
		0.0	$-0.25364547i$	100%	0.0%
4	(1, 1, 1, 2, 2,20)	0.0	0.44073958	100%	0.0%
		0.0	$-0.34899118i$	100%	0.0%

Table 2: Rows 1 and 2 above show the results of calculating a five propagator self-energy loop integral which is of ten variables. Actual integrations are carried out on six and five dimensional integrals after repeating the reductions of variables, and the errors that are provided by Monte Carlo Vegas for each integration are shown in the last column. 3 and 4 are the results without treatments of variable transformation and dimension reductions. D.R. result, which is from the method of dispersion relation, is presented for comparison.

Input parameter	Experimental value
M_Z	(91.1876 ± 0.0021)GeV
Γ_Z	(2.4952 ± 0.0023)GeV
M_W	(80.399 ± 0.023)GeV
Γ_W	(2.085 ± 0.0021)GeV
m_t	(173.2 ± 0.9)GeV
$\Delta\alpha(M_Z)$	(0.05900 ± 0.00033)
$m_b^{\rm MS}$	4.20GeV
$\alpha_s(M_Z)$	0.1184 ± 0.0007
G_μ	$1.16637 \times 10^{-5}\text{GeV}^{-2}$

Table 3: Input parameters and their experimental values, from [38, 39]. The electroweak two-loop corrections of the $Zb\bar{b}$ vertex depend only the first group parameters.

6.2 THE TWO-LOOP CORRECTIONS OF THE WEAK MIXING ANGLE

6.2.1 The corrections to $\sin^2\theta_{\rm eff}^{b\bar{b}}$

The radiative corrections to the effective weak mixing mixing angle, $\sin^2\theta_{\rm eff}^{b\bar{b}}$, as discussed and defined in (2.21) of Section 2.2.2, depend on the parameters as shown in Table 3. One thing that has to be taken carefully is the mass of the W boson. The mass of the Z boson can be measured to a high precision level while the precision test of the W boson mass is larger than that of the Z boson mass one order of magnitude as mentioned in the introduction, so that the uncertainty of the W boson mass has to be considered in our computations. As the mass is fitted to the Breit-Wigner parametrization, as in Eq. (2.17), for the process $e^+e^- \to f\bar{f}$, the actual W mass used in calculations is the $\overline{M}_W$, similar to (5.8), which is slightly smaller than the experimental mass M_W as shown in the discussions of the pole scheme of Section 5.2.3. The factor, $\Delta\alpha$, contributed from the running coupling of the electromagnetism, is used to obtain the renormalized vaccum polization of the photon for the light quarks (except the top quark).

The results in Table 4 show the comparisons of the fermionic two-loop corrections to the weak mixing angle in terms of

$$\Delta\kappa_{b\bar{b}}^{(\alpha^2,\text{ferm})} = \left.\frac{\hat{a}_{\rm f}^{(2)}v_{\rm f}^{(0)}a_{\rm f}^{(0)} - \hat{v}_{\rm f}^{(2)}(a_{\rm f}^{(0)})^2 - (\hat{a}_{\rm f}^{(1)})^2 v_{\rm f}^{(0)} + \hat{a}_{\rm f}^{(1)}\hat{v}_{\rm f}^{(1)}a_{\rm f}^{(0)}}{(a_{\rm f}^{(0)})^2(a_{\rm f}^{(0)} - v_{\rm f}^{(0)})}\right|_{k^2=M_Z^2},$$

which is the next-to-next-leading order term in Eq. (5.10). The table shows the results from different approaches, and it is used as a check for our computations. The results of Ref. [6]

M_W	m_t	$\Delta\kappa_{b\bar{b}}^{(\alpha^2,\mathrm{ferm})} \times 10^3$	
$[GeV]$	$[GeV]$	Ref. [6]	our results
80.399	171.2	−2.278	−2.303
80.399	172.2	−2.331	−2.357
80.399	173.2	−2.386	−2.410
80.399	174.2	−2.441	−2.464
80.399	175.2	−2.496	−2.518
80.422	173.2	−2.402	−2.427
80.445	173.2	−2.418	−2.444

Table 4: Results for the two-loop correction factor $\Delta\kappa_{b\bar{b}}^{(\alpha^2,\mathrm{ferm})}$ to $\sin^2\theta_{\mathrm{eff}}^{b\bar{b}}$, for different values of M_W and m_t. The other input values have been set to $M_Z = 91.1876\,\mathrm{GeV}$, $M_H = 100\,\mathrm{GeV}$, $\Delta\alpha = 0$. The values obtained in this work are compared to that results of Ref. [6].

are given from two methods. One is using the asymptotic expansions for large top-quark mass [24, 5, 41]; the other approach is called Bernstein-Tkachov (BT) method [6, 42]. BT is an algorithm to express the Feynman integrals in terms of a sum of different integrals, which could be more easily integrated than the original one. In Table 4, they indicate that the results for $\sin^2\theta_{\mathrm{eff}}^{b\bar{b}}$ from the MB are consistent with those in [6] up to an error, about 0.25%, due to the uncertainty of the MB integration.

The procedures to obtain those values here for the physical process $Z \to b\bar{b}$ are more complicated than the tests of the scalar integrals presented in the previous section. An important step is to reduce the tensor integrals into scalar ones. As the projections onto the vector and axial-verctor parts of the form factors, like in (5.2), are taken, they could generate hundreds of tensor integrals, which need further manipulations to transform into Mellin-Barnes Integrals. I have implemented this procedure in Mathematica, in the form of an automated algorithm, which performs all the necessary steps, as discussed in Chapters 4 and 5. In order to have an efficient way for the numerical multiple computations, the integrals are separated into two groups, one is called Passarino-Veltman (PV) part in which integrals are calculated in the traditional and more efficient ways, such as what have been discussed in Section 4.3, and the integrals in the other group are computed with the MB, which excels in its generality. In total, over 50 MB integrals have been numerically computed, including all of the iterated integrals due to the crossing poles. The integrated dimensions of the complex integrals range from up to 12 dimensions, which fortunately can be reduced to lower than 6 with the method discussed in Section 4.2. For a six dimension integral, it could take one or two hours to reach an acceptable accuracy. The results from the MB method in Table 4 have indicated a good agreement with the values of other methods. Their differences are also consistent with the errors due to the integration instabilities of the MB integrals, which is under 1%.

M_H [GeV]	$\mathcal{O}(\alpha)$ [10^{-4}]	$\mathcal{O}(\alpha^2)_{\rm ferm}$ [10^{-4}]
100	104.77	1.00
200	100.15	0.71
400	94.397	0.32
600	90.666	0.19
1000	85.748	0.26

Table 5: One-loop and two-loop fermionic corrections to $\sin^2\theta^{b\bar{b}}_{\rm eff}$, with the W-boson mass evaluated from the Standard Model from Ref. [6].

6.2.2 The corrections to R_b

The calculations to the branching ratio R_b, as defined in Section 5.2.4, include not only the radiative corrections to the vector and axial-vector form factors but the QED and QCD corrections to final states of fermions, as discussed in Section 5.2.4. The results are presented in Table 6 with distinct contributions from one- and two-loop corrections. The second column shows the one-loop contribution with the final state QED and QCD corrections (FSR). The main results of this work are listed in the third column for the two-loop fermionic radiative corrections, as added by the FSR of greater than the next leading order, the combined values are shown in the fourth column. The way of including the FSR has been described in (5.12). In addition, owing to the large value of the top-quark mass, the QCD corrections to the ρ parameter, which measures the relative strength of charge and neutral currents, are non-negligible even for higher orders [12, 14]. In the last column, their corrections of the order $\mathcal{O}(\alpha\alpha_s, \alpha\alpha_s^2)$ are shown. In Figure 18, the branching ratio R_b is described as a function of M_H, and the tree-level contribution combined with one-loop, two-loop and higher literally are plotted, as well as the experimental value of R_b with the corresponding one and two confidence levels. Their numerical values are shown in Table 7. The experimental value is $R_b = 0.21629 \pm 0.00066$; its uncertainty is 6.6×10^{-4}, which is comparable to the two-loop corrections. One can tell from the Figure 18 that the dependence on M_H is not strong, and the result including the electroweak two-loop and QCD three-loop corrections is about two confidence level away from the experimental value. The R_b's dependences on M_W and m_t are shown in Figure 19 and **??** with the choice of the Higgs mass, $M_H = 120GeV$. It indicates that the measurements of both masses have reached a high precision level and the small uncertainty is not able to affect the value of R_b. Besides, the fraction including up to two-loop contribution is beyond two confidence level of the experimental value, and it could be an implication of some unknown physics occurring in the Z-boson decay. In addition, our results of R_b have been noticed and get interests by GFitter [43].

M_H [GeV]	$\mathcal{O}(\alpha) + \mathrm{FSR}_{1-\mathrm{loop}}$ $[10^{-3}]$	$\mathcal{O}(\alpha^2_{\mathrm{ferm}})$ $[10^{-4}]$	$\mathcal{O}(\alpha^2_{\mathrm{ferm}}) + \mathrm{FSR}_{>1-\mathrm{loop}}$ $[10^{-4}]$	$\mathcal{O}(\alpha\alpha_s, \alpha\alpha_s^2)$ $[10^{-4}]$
100	-3.632	-6.491	-9.255	-0.404
200	-3.651	-6.495	-9.253	-0.404
400	-3.675	-6.502	-9.253	-0.404
600	-3.690	-6.502	-9.247	-0.404
1000	-3.711	-6.490	-9.227	-0.403

Table 6: Results for electroweak one- and two-loop corrections to R_b, as defined in (5.11), for different values of M_H, The other input values are taken from Table 3, with a fixed value for M_W. Also shown are the effects of two- and three-loop QCD corrections to the final state (fourth column) and to gauge-boson selfenergies (fifth column), Here the "FSR" stands for the final state radiative QCD and QED corrections described by the radiator functions $\mathcal{R}^{(n)}$.

M_H [GeV]	tree-level $+\mathcal{O}(\alpha)$ $+\mathrm{FSR}_{1-\mathrm{loop}}$	$\mathcal{O}(\alpha^2_{\mathrm{ferm}}) + \mathrm{FSR}_{>1-\mathrm{loop}}$ $+\mathcal{O}(\alpha\alpha_s, \alpha\alpha_s^2)$ $[10^{-4}]$	total
100	0.21562	-8.423	0.21478
200	0.21564	-7.984	0.21484
400	0.21565	-7.470	0.21491
600	0.21566	-7.159	0.21494
1000	0.21467	-6.778	0.21500

Table 7: Results for R_b, as in Table 6, but now with M_W calculated from G_μ using the SM prediction. The other input values are taken from Table 3.

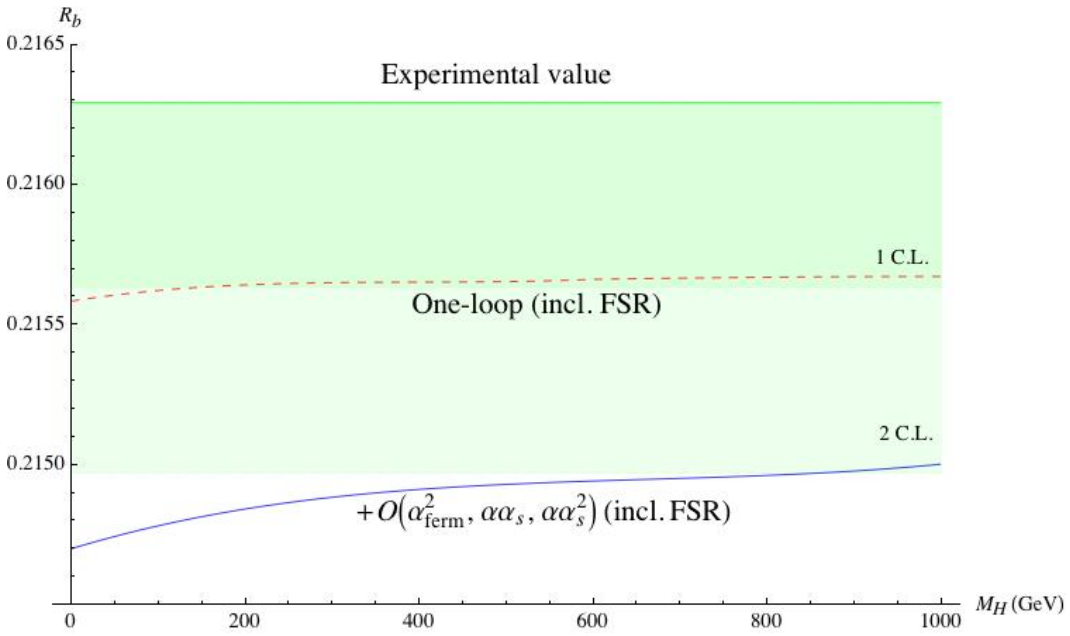

Figure 18: One-loop and two-loop (with QCD three-loop contributions) result for the branching ratio R_b as a function of M_H, and using the SM prediction for M_W to the same order of the perturbation theory. Input values for the other parameters are taken from Table 3. The dark and light green bands correspond to one and two confidence levels respectively to the experimental value of R_b, which is shown as the top edge of the green bands.

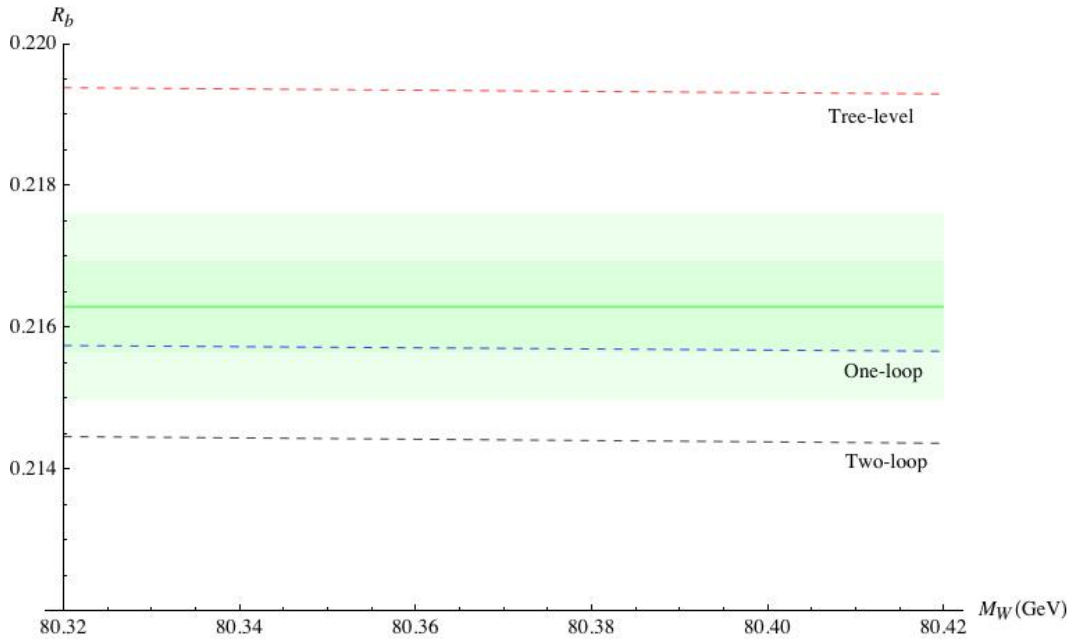

Figure 19: Tree-level, one-loop and two-loop (with QCD three-loop contributions) results for the branching ratio R_b as a function of M_W with $M_H = 120GeV$ are shown as red, blue and black dashed lines. The dark and light green bands correspond to one and two confidence levels respectively to the experimental value of R_b, which is shown as the middle line of the green bands.

7.0 CONCLUSIONS

For the past years, the most celebrated event in high energy physics was the startup of the LHC. It now has reached 4 TeV for each beam energy and two of its four detectors have gone beyond 10^{34} cm^{-1}s^{-1} in luminosity; both pass the highest records of its previous generation counterpart, the Tevatron, which possesses beam energies barely over 1 TeV and a luminosity 4×10^{32} cm^{-1}s^{-1} in its final upgrade. According to the current schedule of the improvement plans, the LHC is expected in 2014 to deliver up to 7 TeV for the beam energies, a collision energy 14 TeV, as well as a luminosity upgrade in 2018. Hence, it would be foreseeable that not only the precision tests of the SM, such as the measurements of the W boson mass and the top-quark mass will be greatly improved but also the evidence of finding the missing part of the SM, the Higgs boson, as well as some unknown physics, could be discovered. Anyhow, the higher accuracy of the measurements, the more computations of two- and three-loop corrections are required to constrain the physical quantities mentioned above.

In this work, the method of the Mellin-Barnes representation for the Feynman integrals is improved in its numerical computations. The improvements include two major steps. The first is to integrate out some of the integration variables by the Mellin convolution theorem; this could be made possible analytically by applying the derived formulas as presented in Chapter 4. Secondly, some modifications are found very useful helping the numerical integrations quickly convergent, like shifting the contours and appropriate variable changes. Each of the two treatments is indispensable; in some difficult integrals, the first could lower the dimension to 5 or 6 complex variables from 10 or 11, and without the latter a MB integral of 4 or 5 dimensions might not converge at all due to the oscillating behavior of the integrands. Another valuable part of this work is the development of a series of programs in Mathematica to generate the MB representation from the original Feynman integrals, to produce the crossing poles as the divergences are isolated, and to reduce the tensor products in the integrals into scalar ones. Combined with the above efforts, we are able to compute the two-loop fermonic radiative corrections of $\sin\theta^{b\bar{b}}_{\rm eff}$ and R_b by calculating up to 6-dimension complex integrals after the analytic treatments mentioned above. The whole computation of the two-loop corrections takes advantages of both of the MB and the PV method to decompose the Feynman integrals into scalar integrals. The MB method could single out the divergences in a general way, though the numerical computations of the complex MB integrals could be slow. The integrals processed from the PV method could be calculated in an efficient way, but the PV method is limited to certain types of the Feynman diagrams. Therefore, we adopt different ways for different Feynman diagrams for a better and quicker convergence of the integrations.

The results of this work for the weak mixing angle $\sin\theta^{b\bar{b}}_{\rm eff}$ are shown to agree with a previous calculation using a different method up to an error which is coming from the numerical error of the integration. As a new result in this thesis, the branching ratio for the bottom quarks, R_b, has been calculated. The results show that its two-loop contributions turns out to be relatively large, and place constraints on the Standard Model and the Higgs mass.

BIBLIOGRAPHY

[1] LEP EWWG Home Page, http://lepewwg.web.cern.ch/LEPEWWG/ .

[2] A. Sirlin, Phys. Rev. D **22**, 971 (1980);
W.J. Marciano and A. Sirlin, Phys. Rev. D **22**, 2695 (1980).

[3] A. Freitas, W. Hollik, W. Walter, and G. Weiglein, Phys. Lett. **B495**, 338 (2000);
A. Freitas, S. Heinemeyer, W. Hollik, W. Walter, and G. Weiglein, Nucl. Phys. Proc. Suppl **89**, 82 (2000).

[4] ATLAS Collaboration, "Detector and Physics Performance Technical Design Report", CERN/LHCC/99-15 (1999);
CMS Collaboration, Technical Design Report, CMS TDR 1-5 (1997/98);
S. Haywood et al., *Electroweak Physics*, hep-ph/0003275, in *Proceedings of the Workshop on Standard model Physics (and more) at LHC*, eds. G. Altarelliand M.L. Mangano (Report CERN 2000-004).

[5] M. Awramik, M. Czakon and A. Freitas, Phys. Rev. Lett. **93**, 201805 (2004);
M. Awramik, M. Czakon and A. Freitas, Phys. Lett. B **642**, 563 (2006);
M. Awramik, M. Czakon and A. Freitas, JHEP **0611**, 048 (2006);
W. Hollik, U. Meier and S. Uccirati, Nucl. Phys. B **731**, 213 (2005);
W. Hollik, U. Meier and S. Uccirati, Nucl. Phys. B **765**, 154 (2007).

[6] M. Awramik, M. Czakon, A. Freitas, and B.A. Kniehl, Nucl. Phys. B, **813**, 174 (2009).

[7] J. Bernabeu, A. Pich and A. Santamaria, Nucl.Phys.B, **363**, 326 (1991).

[8] The LEP Collaborations ALEPH, DELPHI, L3, OPAL, the LEP Electroweak Working Group and the SLD Heavy Flavour and Electroweak Groups
A Combination of Preliminary Electroweak Measurements and Constraints on the Standard Model CERN-EP/2000-016, 21 January 2000.

[9] C. Becchi, A. Rouet, and R. Stora, Ann. Phys. **98**, 287 (1976);
M.Z. Iofa, and I.V. Tyutin, Theor. Math. Phys. **27**, 316 (1976).

[10] D. Bardin et al., Comput.Phys.Commun., **133**, 229 (2001);
A.B. Arbuzov et al., Comput.Phys.Commun., **174**, 728 (2006).

[11] Gfitter Group, Gfitter web page, http://cern.ch/Gfitter;
H. Flaecher et al., Eur.Phys.J.C, **60**, 728 (2006).

[12] A. Djouadi, and C. Verzegnassi, Phys. Lett. B, **195**, 265 (1987);
A. Djouadi, Nuovo Cim. A, **100**, 357 (1988);
B.A. Kniehl, Nucl. Phys. B, **347**, 86 (1990);
B.A. Kniehl,and A. Sirlin, Nucl. Phys. B, **371**, 141 (1992);
A. Djouadi, and P. Gambino, Phys. Rev. D, **49**, 3499 (1994).

[13] ALEPH Collaboration, L3 Collaboration, OPAL Collaboration, SLD Collaboration, the LEP Electroweak Working Group, the SLD Electroweak and Heavy Flavor Groups, Phys.Rept., **427**, 257 (2006).

[14] L. Avdeev, J. Fleischer, S. Mikhailov, and O. Tkachov, Phys. Lett. B, **336**, 560 (1994);
K.G. Chetyrkin, J.H. Kuhn, and M. Steinhauser, Phys. Lett. B, **351** 331 (1995);
K.G. Chetyrkin, J.H. Kuhn, and M. Steinhauser, Phys. Rev. Lett., **75** 3394 (1995).

[15] J.J. van der Bij, K.G. Chetyrkin, M. Faisst, and T. Seidensticker, Phys. Lett. B, **498**, 156 (2001);
M. Faisst, J.H. Kuhn, T. Seidensticker, and O. Veretin, Phys. Lett. B, **665**, 649 (2003);
R. Boughezal, J.B. Tausk, and J.J. van der Bij, Phys. Lett. B, **713**, 278 (2005);
R. Boughezal, J.B. Tausk, and J.J. van der Bij, Phys. Lett. B, **725**, 3 (2005);
K.G. Chetyrkin, J.H. Kuhn, and M. Steinhauser, Phys. Rev. Lett., **482** 213 (1996);
Y. Schroder, and M. Steinhauser, Phys. Lett. B, **622** 124 (2005);
K.G. Chetyrkin, M. Faisst, J.H. Kuhn, P. Maierhoefer, and C. Sturm, Phys. Rev. Lett., **97** 102003 (2006);
R. Boughezal, and M. Czakon, Nucl. Phys. B, **755**, 221 (2006).

[16] A. Straessner, talk given at the *XXXVth Rencontres de Moriond*, Les Arcs, March 2000, to appear in the proceedings.

[17] THe LEP working group for Higgs boson searches, P. Bock et al., CERN-EP/2000-055.

[18] M. Bohm, W. Hollikand H. Spiesberger, Fortschr. Phys., **34**, 687 (1986);
M. Bohm and A. Denner in : M.A. Perez, R Huerta, *Proc. of the Workshop on High Energy Phenomenology*, Work Scientific, Singapore, (1992).

[19] A. Denner Fortschr. Phys., **41**, 307 (1993);
W. Hollik, *Renormalization of the Standard Model*, in P. Langacker: *Precision Tests of the Standard Electroweak Model* (Advanced Series on Directions in High Energy Physics, Vol 14), Work Scientific, Singapore, (1995).

[20] S. Bauberger, doctoral thesis, der Universitat Wurzburg, (1997).

[21] A. Freitas, W. Hollik, W. Walter, and G. Weiglein, Nucl. Phys., **B632**, 189 (2002).

[22] S. Bauberger, F. A. Berends and M. Buza, Nucl. Phys. B, **434**, 383 (1995).

[23] M. Beneke and V. A. Smirnov, Nucl. Phys. B, **522**, 321 (1998).

[24] V. A. Smirnov, Applied Asymptotic Expansions in Momenta and Masses (STMP **177**, Springer, Berlin, Heidelberg 2002).

[25] K. G. Chetyrkin and F. V. Tkachov, Nucl. Phys. B, **192**, 159 (1981);
S. Laporta, Int.J.Mod.Phys.A, **15**, 5087 (2000);
C. Anastasiou and A. Lazopoulos, JHEP, **0407**, 046 (2004);
U. Aglietti and A. Bonciani, Nucl. Phys. B, **668**, 3 (2003).

[26] T. Binoth and G. Heinrich, Nucl. Phys. B, **585**, 741 (2000);
T. Binoth and G. Heinrich, Nucl. Phys. B, **680**, 375 (2004).

[27] C. Anastasiou and R. Daleo, JHEP, **0610**, 31 (2006);
M. Czakon, Comput.Phys.Commun, **175**, 559 (2006).

[28] *Table of Integrals, Series, and Products*, eds. I.S. Gradshteyn, I.M. Ryzhik, and A. Jeffrey, Academic Press, (1994).

[29] G.P. Lepage, Journal of Computational Physics, **17**, 192 (1978);
G.P. Lepage, Cornell preprint CLNS, 80 (1980).

[30] T. Hahn, Comput.Phys.Commun., **140**, 418 (2001);
T. Hahn and C. Schappacher, Comput.Phys.Commun., **143**, 54 (2002).

[31] R. Mertig, M. Bohm and A. Denner, Comput.Phys.Commun., **64**, 345 (1991).

[32] S. Willenbrock, and G. Valencia, Phys. Lett. B **259**, 373 (1991);
A. Sirlin, Phys. Rev. Lett. **67**, 2127 (1991);
R.G. Stuart, Phys. Lett. B **262**, 113 (1991).

[33] H. Veltman, Z. Phys. C **62**, 35 (1994).

[34] M. Passaera, and A. Sirlin, Phys. Rev. D **58**, 113010 (1998);
P. Gambino, and P.A. Grassi, Phys. Rev. D **62**, 076002 (2000);
A.R. Bohm, and N.L. Harsman, Nucl. Phys. B **581**, 91 (2000).

[35] D.Y. Bardin, A. Leike, T. Riemann and M. Sachwitz, Phys. Lett. B, **206**, 546 (1988).

[36] K.G. Chetyrkin, A.L. Kataev, and F.V. Tkachov, Phys. Lett. B, **85**, 277 (1979);
M. Dine, and J.R. Sapirstein, Phys. Rev. Lett., **43** 668 (1979);
W. Celmaster, and R.J. Gonsalves, Phys. Rev. Lett., **44** 560 (1980);
S.G. Gorishnii, A.L. Kataev, and S.A. Larin, Phys. Lett. B, **212**, 238 (1988);
K.G. Chetyrkin, and J.H. Kuhn, Phys. Lett. B, **248** 359 (1990);
S.G. Gorishnii, A.L. Kataev, and S.A. Larin, Phys. Lett. B, **259**, 144 (1991);
L. R.. Surguladze, and M.A. Samuel, Phys. Rev. Lett., **66** 560 (1991);
A.L. Kataev, Phys. Lett. B, **287** 209 (1992);
K.G. Chetyrkin, Phys. Lett. B, **307** 169 (1993).

[37] K.G. Chetyrkin, J. Kuhn, and A. Kwiatkowski, in *Reports of the Working Group on Precision Calculations for the Z resonance*, eds. D. Bardin, W. Hollik, and G. Passarino, report CERN, **95-03**, 175-263 (1995).

[38] K. Nakamura *et al.* [Particle Data Group], J. Phys. G, **37**, 075021 (2010);

[39] Tevatron Electroweak Working Group and for the CDF and D0 Collaborations, arXiv:1107.5255 [hep-ex];
H. Burkhardt, and B. Pietrzyk Phys. Rev. D, **84**, 037502 (2011);

[40] E.M. Peskin, and D.V. Schroeder, *An Introduction to Quantum Field Theory*, Addison-Wesley, (1995).

[41] V.A. Smirnov, *Evaluating Feynman Integrals*, Springer Tracts Mod. Phys., 211 (2004).

[42] F.V. Tkachov, Nucl. Instrum. Meth. A, **389**, 309 (1997); D.Yu. Bardin, L.V. Kalinovskaya, and F.V. Tkachov, in *Proceedings of the 15th International Workshop on High-Energy Physics and Quantum Field Theory*(QFTHEP2000), Tver, Russia, 14-20 September 2000, arXiv:hep-ph/0012209;
G. Passarino, Nucl. Phys. B, **619**, 257 (2001), arXiv:hep-ph/0108252;
A. Ferroglia, M. Passera, G. Passarino, and S. Uccirati, Nucl. Phys. B, **650**, 162 (2003), arXiv:hep-ph/0209219;
A. Ferroglia, M. Passera, G. Passarino, and S. Uccirati, Nucl. Phys. B, **680**, 199 (2004), arXiv:hep-ph/0311186;
S. Actis, A. Ferroglia, G. Passarino, M. Passera, and S. Uccirati, Nucl. Phys. B, **703**, 3 (2004), arXiv:hep-ph/0402132;
G. Passarino, and S. Uccirati, Nucl. Phys. B, **747**, 113 (2006), arXiv:hep-ph/0603121;
G. Passarino, C. Sturm, and S. Uccirati, Phys. Lett. B, **655**, 298 (2007), arXiv:hep-ph/0707.1401.

[43] D. Kennedy, talk in LoopFest XI 2012, http://gfitter.desy.de/talks.html.